

2013

Residual Stresses Due to Circumferential Girth Welding of Austenitic Stainless Steel Pipes

Farzan Tarak
Lehigh University

Follow this and additional works at: <http://preserve.lehigh.edu/etd>



Part of the [Mechanical Engineering Commons](#)

Recommended Citation

Tarak, Farzan, "Residual Stresses Due to Circumferential Girth Welding of Austenitic Stainless Steel Pipes" (2013). *Theses and Dissertations*. Paper 1649.

This Thesis is brought to you for free and open access by Lehigh Preserve. It has been accepted for inclusion in Theses and Dissertations by an authorized administrator of Lehigh Preserve. For more information, please contact preserve@lehigh.edu.

Residual Stresses Due to Circumferential Girth Welding of Austenitic
Stainless Steel Pipes

By

Farzan Tarak

A Thesis

Presented to the Graduate and Research Committee

of Lehigh University

in Candidacy for the Degree of

Master of Science

in

Mechanical Engineering

Lehigh University

May 2013

This thesis is accepted and approved in partial fulfillment of the requirements for the Master of Science.

Date

Dr. Herman F. Nied, Thesis Advisor

Dr. D. Gary Harlow, Chairperson
Mechanical Engineering and Mechanics

Acknowledgements

I would never have been able to finish my thesis without the guidance of Professor Herman f. Nied, help from friends, and support from my family and wife.

I would like to express my deepest gratitude to my advisor, Professor Herman F. Nied, for his excellent guidance, caring, patience, and providing me with an excellent atmosphere for doing research.

Furthermore, I would like to thank ESI Group for providing ESI Visual-Environment and SYSWELD software for Lehigh University to complete this study.

I would like to thank my mother and sister for their kindness and their support. They were always supporting me and encouraging me with their best wishes.

Finally, I would like to give my love and special thanks to my wife, Elham Takin, for her unexpressed supports and encouragements.

Table of Contents

Acknowledgements	i
Table of Figures	v
Abstract.....	1
1 Introduction	2
1.1 Arc Welding	5
1.1.1 Shield Metal Arc Welding (SMAW).....	6
1.1.2 MIG/MAG or Gas Metal Arc Welding (GMAW).....	7
1.1.3 Submerged Arc Welding (SAW).....	9
1.1.4 TIG/GTAW Welding.....	10
1.1.5 Plasma Arc Welding (PAW).....	14
1.2 Effects of Welding	14
1.2.1 Thermal and Heat Flow	15
1.2.2 Metallurgy.....	18
1.2.3 Mechanical Effects	22
1.3 Welding Simulation Process (Literature Review).....	24
2 Welding Simulation	26
2.1 Heat Transfer Modeling of Arc Welding	26
2.2 Heat Source Modeling.....	29
3 Numerical and Computational Modeling of Circumferential Pipe Welding Using ESI Visual-Weld	31
3.1 Geometry and Material Properties	32
3.2 Axisymmetric 2-D Modeling of Pipe Girth Welding.....	34
3.2.1 Geometry of the Welded Components.....	35
3.2.2 Axisymmetric Meshed Model.....	35
3.2.3 Boundary Conditions and Clamping	36
3.2.4 Thermal Analysis and Results.....	37
3.2.5 Residual Stress Analysis and Results	39

3.3	Shell Modeling of Pipe Girth Welding.....	41
3.3.1	Thermal Analysis and Results.....	43
3.3.2	Residual Stress Analysis and Results	45
3.4	3-D Modeling of Circumferential Girth Welding of Pipe	47
3.4.1	Thermal analysis and results	48
3.4.2	Residual Stress Analysis and Results	49
4	Final Results and Discussions	52
5	Conclusion and Future Works	62
6	References	64
	Appendix A.....	66
	Script Used in SYSWELD for Defining the Heat Source.....	66
	Appendix B	74
	Script Used in SYSWELD for Defining Mechanical Properties.....	74
	Vita	77

Table of Figures

Exhibit 1-1 SHIELDED METAL ARC WELDING (SMAW) [7]	7
Exhibit 1-2 Typical GMAW Semiautomatic Setup with Voltage-Sensing Feeder [8].....	9
Exhibit 1-3 TIG welding [10]	12
Exhibit 1-4 Typical GTAW Welding System [10].....	13
Exhibit 1-5 Interrelated physical phenomenon in computation of heat treatment, arc welding analysis and simulation, prepared by ESI Group for SYSWELD [13]	15
Exhibit 1-6 Heat source efficiencies in different welding methods. Reprinted from Kou [14]	16
Exhibit 1-7 Cross section of welding showing areas representing contributions from base metal and filler metal [14].....	17
Exhibit 1-8 Milting efficiency: (a) lower at lower heat input and welding speed; (b) higher at higher heat input and welding speed [14].....	17
Exhibit 1-9 Softening of work-hardened material caused by welding: (a) thermal cycles; (b) strength or hardness profile Reprinted from Kou [14].....	19
Exhibit 1-10 Yield strength profiles across welds of two work-hardened 5083 aluminum plates. Reprinted from Kou [14]	19
Exhibit 1-11 Grain growth in HAZ: (a) Phase diagram; (b) Thermal cycles; (c) Grain size variations. Reprinted from Kou [14]	20
Exhibit 1-12 Effect of heat input per unit length of weld on: (a) width of HAZ (shaded); (b) Thermal cycles near fusion boundary, and (c) Strength or hardness profiles. Reprinted from Kou [14]	21
Exhibit 1-13 Effect of heat input per unit length of weld on HAZ hardness in a work-hardened 5356 aluminum. Reprinted from Kou [14].....	21
Exhibit 1-14 Demonstration of thermal residual stresses by three-bar arrangement: (a) during heating; (b) during cooling	22
Exhibit 1-15 Typical distribution of longitudinal (σ_x) and transverse (σ_y) residual stresses in but weld. Reprinted from Kou [14]	23
Exhibit 1-16 Typical distortion in welded parts. Reprinted from Kou [14].....	24
Exhibit 2-1 Goldak's Double ellipsoidal Model of arc welding heat source.....	30
Exhibit 3-1 Half plane 3-D modeling of girth welding of pipe.....	33
Exhibit 3-2 Welding direction and start point.....	33
Exhibit 3-3 Geometry of Axisymmetric 2-D model of Pipe Welding.....	35
Exhibit 3-4 Meshed axisymmetric 2-D model of a welded pipe.....	36
Exhibit 3-5 Clamping condition and symmetric plane of axisymmetric model.....	36
Exhibit 3-6 Temperature field after passing of the heat source $^{\circ}C$	37
Exhibit 3-7 Nodal Temperature ($^{\circ}C$) at the center of weld line from top to bottom in different time ($t=1s$ is the passing time of heat source from the section).....	38
Exhibit 3-8 Nodal Temperature ($^{\circ}C$) in axial direction at the outside surface of pipe	39
Exhibit 3-9 Axial stress field in axisymmetric modeling of pipe girth welding (MPa).....	40
Exhibit 3-10 Hoop stress field in axisymmetric modeling of pipe girth welding (MPa).....	40
Exhibit 3-11 von Mises stress field in axisymmetric modeling of pipe girth welding (MPa)	41

Exhibit 3-12 Shell modeling and its geometry.....	42
Exhibit 3-13 Clamping Condition of shell model	43
Exhibit 3-14 Temperature Contour ($^{\circ}C$) during welding at time $t = 25.5s$	44
Exhibit 3-15 Nodal temperature profile ($^{\circ}C$) at the surface of shell in axial direction.....	45
Exhibit 3-16 Axial Stress in shell modeling of pipe girth welding (MPa).....	46
Exhibit 3-17 Hoop Stress in Cylindrical coordinate in shell modeling of pipe girth welding (MPa)	46
Exhibit 3-18 17 von Mises Stress distribution in shell modeling of pipe girth welding (MPa).....	47
Exhibit 3-19 Temperature distribution $^{\circ}C$ during welding at time $t = 25.5$	49
Exhibit 3-20 Distribution of Axial Stresses in 3-D simulation of girth welding of pipe (MPa)	50
Exhibit 3-21 Hoop residual stress distribution in cylindrical coordination (MPa).....	51
Exhibit 4-1 Comparison of axial stresses at the inside surface of the pipe.....	53
Exhibit 4-2 Comparison of axial stresses at the outside surface of the pipe	54
Exhibit 4-3 Comparison of hoop stresses at the inside surface of the pipe.....	56
Exhibit 4-4 Comparison of hoop stresses at the outside surface of the welded pipe.....	57
Exhibit 4-5 Comparison of von Mises stresses at the inside surface of the welded pipe	58
Exhibit 4-6 Comparison of von Mises stresses at the outside surface of the welded pipe.....	59
Exhibit 4-7 influence of clamping condition on axial residual stress in 2-D axisymmetric modeling.....	61

Abstract

Welding, as a joining method in fabrication of engineering products and structural elements, has a direct influence on thermo-mechanical behavior of components in numerous structural applications. Since these thermo-mechanical behaviors have a major role in the life of welding components, predicting thermo-mechanical effects of welding is a major factor in designing of welding components. One of the major of these effects is generation of residual stresses due to welding. These residual stresses are not the causes of failure in the components solely, but they will add to external loads and stresses in operating time. Since, experimental methods are time consuming and expensive, computational simulation of welding process is an effective method to calculate these residual stresses. This investigation focuses on the evaluation of residual stresses and distortions due to circumferential girth welding of austenitic stainless steel pipes using the commercial finite element software ESI Visual-Environment and SYSWELD® to simulate welding process. Of particular importance is the comparison of results from three different types of mechanics models: 1) Axisymmetric, 2) Shell, and 3) Full 3-D.

1 Introduction

Welding, as a joining method in fabrication of engineering products and structural elements, has a direct effect on thermo-mechanical behavior of components in numerous structural applications. For example, the influence of welding is of great importance in fatigue behavior and fracture in the heat-affected zone of welding pipes. Due to the high temperatures generated during welding in the Heat Affected Zone (HAZ), as well as phase transformation in the melting zone following rapid solidification and cooling, undesirable residual stresses and distortions are generated in welded components. It is essential to simulate the welding process to better understand and predict the mechanical and thermal behavior of welded components. There are two major methods of determining residual stresses, experimental methods and computerized simulations methods. Experimental methods can be divided into destructive and non-destructive methods. Diffraction methods are an example of non-destructive methods [1]. Nowadays, due to advancements in finite element analysis software along with powerful personal computers equipped with high performance and high speed CPUs, computerized simulation methods are more efficient, accurate, convenient, and significantly decrease the cost of simulation over experimental methods. Perhaps of even greater importance, is that computer simulations permit the engineer to better visualize the complex cause and effect relationships that exist between the various welding parameters and the final residual stresses. Prediction of residual stresses is particularly important for applications in nuclear, aerospace, defense, and automotive industries.

Residual stresses are of special significance in pressure vessels and pipelines in situations where they are designed with lower safety factors [2]. Welding generally causes high tensile stresses, as high as yield stress, along with compressive stresses in the welding components [2]. Residual stresses may cause early failure in welded components by causing early crack

nucleation and accelerating fatigue, stress corrosion cracking, fracture, and undesirable deformation in the components [2]. The residual stresses due to welding are “frozen” in the components and are always in a state of balanced equilibrium within the welded joints. This means that when an area of a component is under compressive residual stress, the neighboring area is subjected to tensile residual stresses. Although most components do not fail merely due to the residual stresses, they add to stresses from external loads. Hence, residual stresses usually tend to lessen the strength of the welded component [3]. Therefore, it is necessary to predict these kinds of residual stresses for designing welded structures and products in order to prevent unexpected and premature failures.

The circumferential girth weld is the major type of joint in most piping systems. If the wall thickness is great, it is usually necessary to use multi-passes welding. A good estimation of the welding residual stresses is needed, especially when risk of a crack growth is critical in piping systems, i.e. piping systems in nuclear reactors. In this case, the welding stresses contribute significantly to the total stress field, in addition to the anticipated design loads such as internal pressure and support reactions. The magnitude and distribution of welding residual stresses are highly dependent on clamping situation and boundary conditions, i.e. structural restraints. In addition, the ratio of wall thickness over diameter, the magnitude of heat input, and the number of weld passes and sequence are important [4]. Since welding residual stresses are primarily the result of volume changes during solidification, the stresses can be accurately expressed in terms of the three principal stresses in cylindrical coordinate, σ_{zz} axial stress, $\sigma_{\theta\theta}$ hoop stress, σ_{rr} radial stress, which are traditionally considered in the study of residual stresses in circumferential girth pipe welding.

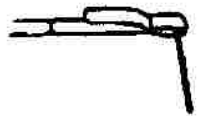
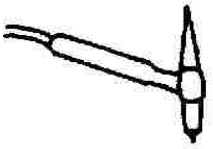

In large diameter pipes with thin wall thickness (low ratio of thickness/diameter), a more or less uniform temperature can be assumed through the pipe thickness during circumferential girth welding. In this case, the primary deformation from thermal stresses after welding is the circumferential strain due to radial contraction in the cooling weld metal. After completion of the cooling process, this radial contraction, along with the cross sectional symmetry condition can be expected to result in an almost linear axial stress variation (bending) through pipe wall thickness with tensile axial stresses at the inner surface, and compressive axial stresses on the outer surface. Based on the information given by Brickstad et al [4], the corresponding hoop stresses are typically tensile all through wall thickness and almost have the same magnitude of as the maximum axial stress if the yield strength of the filler and the base materials are the same [4]. These results are the same as early analytical solutions from elastic shell theory, such as given by Timoshenko, et al [5].

In pipes with large wall thicknesses (high ratio of thickness/diameter), the evolution of the residual stresses is much more complex, primarily due to non-uniformity of temperature gradients through the wall thickness during welding. The magnitude of the tensile axial stress at the inner surface is almost as magnitude as yield stress and large zone of tensile axial stresses exist near the inner surface, as Brickstad et al [4]stated.

In the present study, a procedure for creating axisymmetric 2-D, shell, and fully 3-D models of circumferential girth welding, using the commercial finite elements software, ESI Visual-Environment and SYSWELD, is described in order to determine welding residual stresses.

1.1 Arc Welding

Arc welding is a type of welding that uses a welding power supply to create an electric arc between an electrode and the base material to melt the metals at the welding point. The output voltage could either be DC or AC and divided in two category, consumable and non-consumable electrode. Consumable electrode arc welding is such as Shielded Metal Arc Welding (SMAW), Gas Metal Arc Welding (GMAW), which both are Flux Cored Arc Welding (FCAW), Submerged Arc Welding (SAW), Electro-gas Welding (EGW), and Electro-slag Welding (ESW). Non-consumable electrode arc welding is like Gas Tungsten Arc Welding (GTAW), and Plasma Arc Welding. Table 1-1 shows these methods of welding and their specifications.

Welding Process	AWS Designation	Electrode	Shielding Gases	Remarks
Shielded Metal Arc Welding (also known as “stick” welding)	SMAW 	Consumable Stick Electrode	Some shielding. Gas produced from welding rod.	Common in the field and in small shops. Produces excessive fumes.
Gas Tungsten Arc Welding	GTAW 	Non Consumable Tungsten Electrode	Argon most common gas. Helium used for penetrating welds	Relatively clean process
Gas Metal Arc Welding	GMAW 	Consumable Wire Electrode	Argon, CO ₂ , and CO ₂ /Ar are typical	Metal flows across arc from electrode to work piece



Flux Core Arc Welding	FCAW 	Consumable Wire Electrode with Flux Core	External (e.g. CO ₂) or flux generated gas	Variation of GMAW
Plasma Arc Welding	PAW 	Non Consumable Tungsten Electrode	Argon and Others	Three principal modes: melt-in, keyhole, and needle arc

Table 1-1 Arc Welding Processes [6]

1.1.1 Shield Metal Arc Welding (SMAW)

Shield Metal Arc Welding (SMAW) is a welding method that joints metals by heating them with an arc between a coated metal electrode and the base. The electrode outer coating, called flux, assists in creating the arc and provides the shielding gas and slag covering to protect the weld from contamination. The electrode core provides most of the weld filler metal. When the electrode is moved along the workpiece at the correct speed the metal deposits in a uniform layer called a bead. The Stick welding power source provides constant current (CC) and may be either alternating current (AC) or direct current (DC), depending on the electrode being used. The best welding characteristics are usually obtained using DC power sources. The power in a welding circuit is measured in voltage and current. The voltage (Volts) is governed by the arc length between the electrode and the base and is influenced by electrode diameter. Current is a more practical measure of the power in a weld circuit and is measured in amperes (Amps). The amperage needed to weld depends on electrode diameter, the size and thickness of the pieces to be welded, and the position of the welding. Thin metals require less current than thick metals, and a small electrode requires less amperage than a large one. It is preferable to weld on work in

the flat or horizontal position. However, when forced to weld in vertical or overhead positions it is helpful to reduce the amperage from that used when welding horizontally. Best welding results are achieved by maintaining a short arc, moving the electrode at a uniform speed, and feeding the electrode downward at a constant speed as it melts [7].

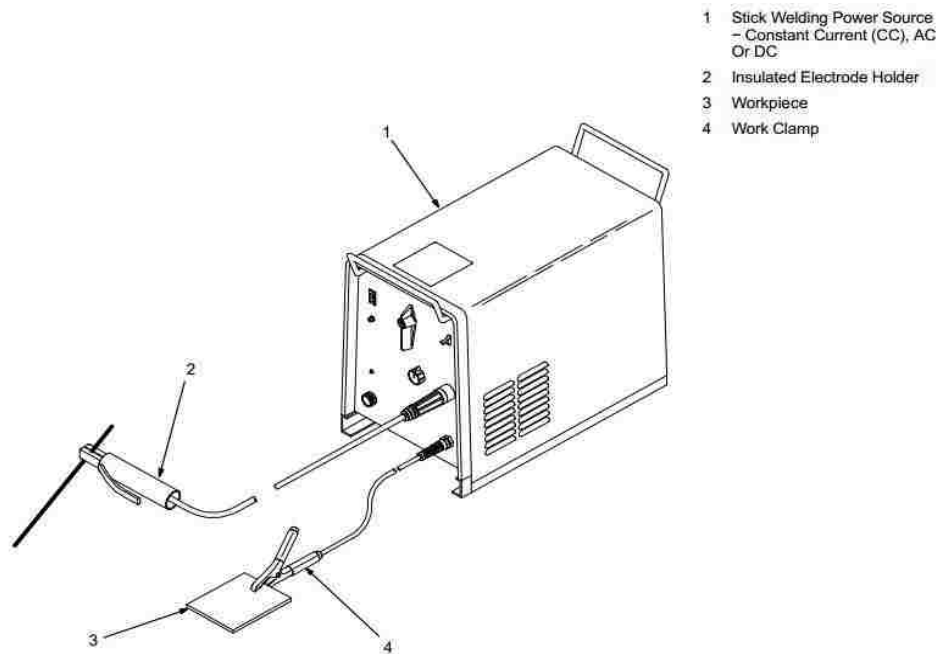


Exhibit 1-1 SHIELDED METAL ARC WELDING (SMAW) [7]

1.1.2 MIG/MAG or Gas Metal Arc Welding (GMAW)

MIG (Metal Inert Gas) or MAG (Metal Active Gas) welding also called Gas Metal Arc Welding (GMAW) is a welding process which joins metals by heating the metals to their melting point with an electric arc. The arc is between a continuous, consumable electrode wire and the metal being welded. The arc is shielded from contaminants in the atmosphere by a shielding gas. GMAW can be done in three different ways, Semiautomatic Welding, Automatic Welding, and Machine Welding. Basic equipment for a typical GMAW semiautomatic setup:

- Welding Power Source

- Wire Feeders (Constant Speed And Voltage-Sensing)

Constant Speed Feeder - Used only with a constant voltage (CV) power source. This type of feeder has a control cable that will connect to the power source. The control cable supplies power to the feeder and allows the capability of remote voltage control with certain power source/feeder combinations. The wire feed speed (WFS) is set on the feeder and will always be constant for a given preset value.

Voltage-Sensing Feeder - Can be used with either a constant voltage (CV) or constant current (CC) - direct current (DC) power source. This type of feeder is powered off of the arc voltage and does not have a control cord. When set to (CV), the feeder is similar to a constant speed feeder. When set to (CC), the wire feed speed depends on the voltage present. The feeder changes the wire feed speed as the voltage changes. A voltage sensing feeder does not have the capability of remote voltage control.

- Supply of Electrode Wire.
- Welding Gun - delivers electrode wire and shielding gas to the weld puddle.
- Shielding Gas Cylinder - provides a supply of shielding gas to the arc. [8]

- 1 Constant Voltage (CV) Welding Power Source
- 2 Contactor Control/Power Cord
- 3 Weld Cable To Feeder
- 4 Ground Cable To Workpiece
- 5 Workpiece
- 6 Welding Gun
- 7 Constant Speed Wire Feeder
- 8 Electrode Wire
- 9 Gas Hose
- 10 Shielding Gas Cylinder

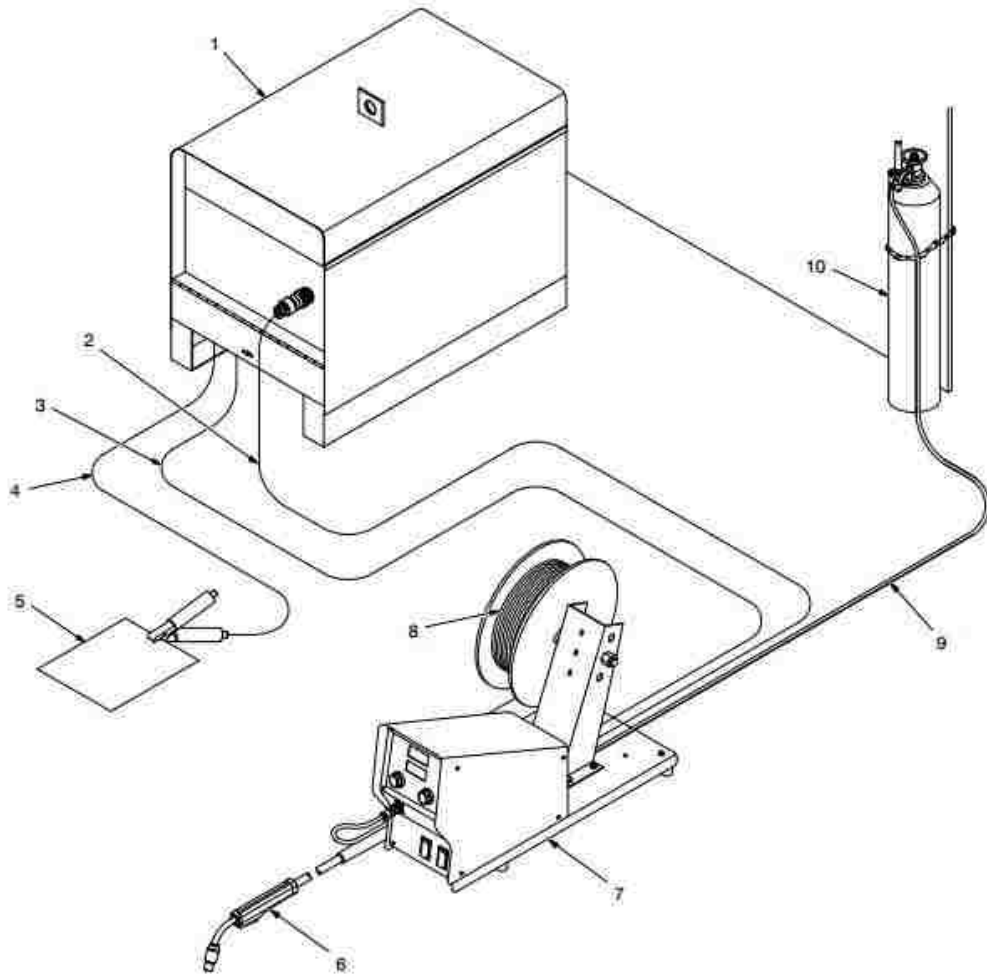


Exhibit 1-2 Typical GMAW Semiautomatic Setup with Voltage-Sensing Feeder [8]

1.1.3 Submerged Arc Welding (SAW)

Submerged Arc Welding (SAW) is a unique welding process because the welding zone (arc and molten metal) has been shielded by a blanket of granular and fusible flux. This welding method just performs as Automatic and Semiautomatic Sub Arc. It has some advantages such as:

- Higher deposition enhances welding speed or production
- Deep penetration in some cases may eliminate joint preparation.
- Excellent mechanical properties for high quality code and X-Ray requirements.
- Improves welding operator comfort and appeal.

There are some notifications must be considered about usage of Submerged Arc Welding for welding of stainless steel. Submerged arc is not widely used on stainless steel because of the high heat input from the Submerged Arc process. In 80 percent of stainless steel applications, submerged arc welding uses for carbon steel. Austenitic stainless has a higher thermal coefficient of expansion, and a lower thermal conductivity and mild steel. A high input will enhance chances of carbide precipitation and distortion.

Ferritic and martensitic stainless steel can be welded by Submerged Arc Welding, but has not gained the acceptance that Gas Tungsten Arc, Gas Metal Arc and Shielded Metal Arc has found. Submerged Arc welding method usually uses in stainless cladding rather than welding because it has a wide and unique fusion pattern, but a shallow penetration [9].

1.1.4 TIG/GTAW Welding

TIG (Tungsten Inert Gas) welding or Gas-Shielded Tungsten Arc Welding (GTAW) is a process that produces an electric arc maintained between a non-consumable tungsten electrode and the part to be welded. The heat-affected zone, the molten metal, and the tungsten electrode are all shielded from atmospheric contamination by a blanket of inert gas fed through the GTAW torch. In some cases, Hydrogen gas may be added to enhance travel speeds. The GTAW process can produce temperatures of up to 35,000° F (19,426°C). The torch contributes heat only to the

base metal. If filler metal is required to make the weld, it may be added manually in the same manner as it is added in the oxyacetylene welding process, or in other situations may be added using a cold wire feeder.

GTAW is used to weld steel, stainless steel, nickel alloys such as Monel® and Inconel®, titanium, aluminum, magnesium, copper, brass, bronze, and even gold. GTAW can also weld dissimilar metals to one another such as copper to brass and stainless steel to mild steel. Other advantages of GTAW welding:

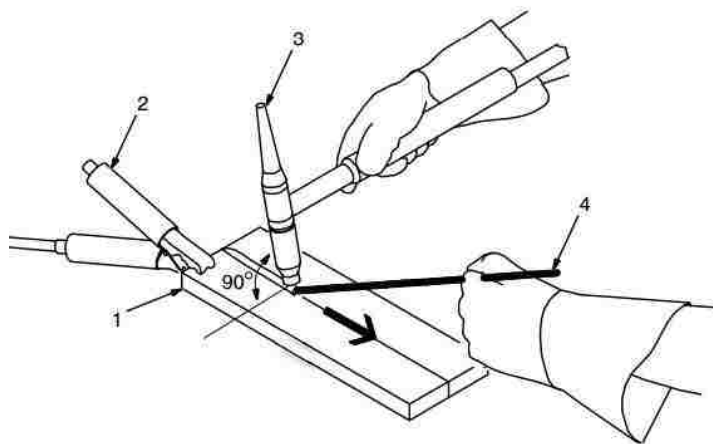
- Concentrated Arc - Permits pinpoint control of heat input to the base metal resulting in a narrow heat-affected zone.
- No Slag - No requirement for flux with this process; therefore no slag to obscure the welder's vision of the molten weld pool.
- No Sparks or Spatter - No transfer of metal across the arc. No molten globules of spatter to contend with and no sparks produced if material being welded is free of contaminants.
- Little Smoke or Fumes - Compared to other arc-welding processes like stick or flux cored welding, few fumes are produced.
- Welds more metals and metal alloys than any other arc welding process.
- Good for welding thin material.
- Good for welding dissimilar metals together.

Disadvantages of GTAW welding:

- Slower travel speeds than other processes.

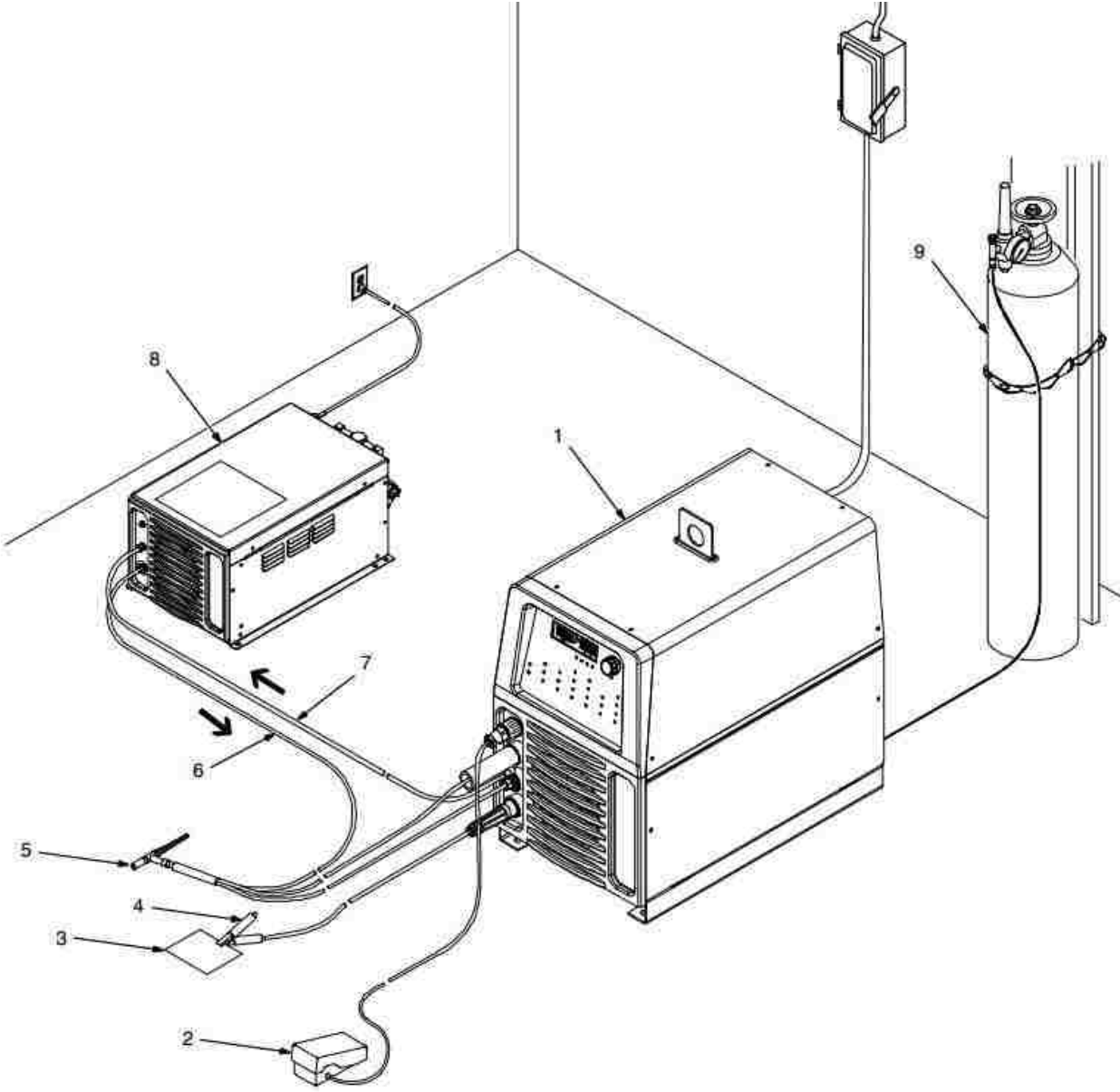
- Lower filler metal deposition rates.
- Hand-eye coordination is a required skill.
- Brighter UV rays than other processes.
- Equipment costs can be higher than with other processes.
- Concentrations of shielding gas may build up and displace oxygen when welding in confined areas [10].

Exhibit 1-3 TIG welding [10]



- 1- Base metal
- 2- Work clamp
- 3- Torch
- 4- Filler Rod

Exhibit 1-4 Typical GTAW Welding System [10]



- 1 Welding Power Source – Constant Current (CC)
- 2 Foot Control
- 3 Workpiece

- 4 Work Clamp
- 5 Torch
- 6 Coolant Out Hose

- 7 Coolant In Hose
- 8 Cooling System
- 9 Shielding Gas

1.1.5 Plasma Arc Welding (PAW)

PAW (Plasma Arc Welding) is a process, which is very similar to TIG welding. It is a development of the TIG method, which is designed to increase productivity.

In PAW, there are two separate gas flows, the plasma gas which flows round the tungsten electrode and subsequently forms the core of the plasma arc and the shielding gas which provides protection for the molten pool. PAW is used in three modes:

1. Micro-plasma welding, with welding current from 0.1A to 20A.
2. Medium-plasma welding, with welding current from 20A to 100A.
3. Keyhole welding, above 100A, where the plasma arc penetrates the wall thickness.

It is widely used for high-quality joints in the aerospace, process, chemical and petroleum industries [11].

1.2 Effects of Welding

Arc welding is an interrelated physical phenomenon and multi-field interaction, which includes heat transfer, magnetism, electricity, chemical composition, etc. Exhibit 1.5 prepared by ESI Group for simulation of heat treatment and welding, shows how these different fields are coupled in welding analysis. The modeling of CFD and Fluid Flow is not included in Exhibit 1.5, because the effect of the fluid flow on the deformation and stress field can be considered as negligible [12].

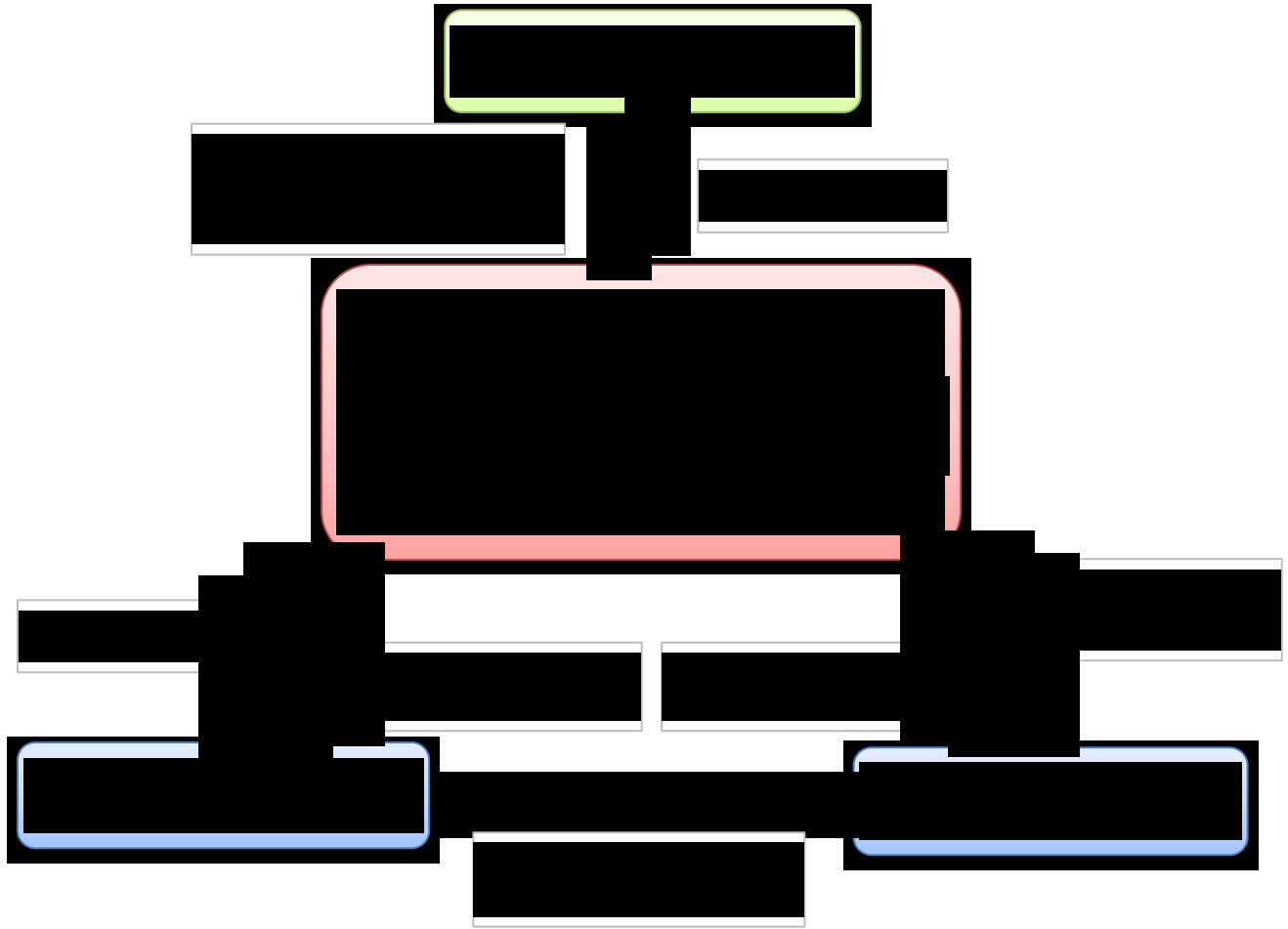


Exhibit 1-5 Interrelated physical phenomenon in computation of heat treatment, arc welding analysis and simulation, prepared by ESI Group for SYSWELD [13]

1.2.1 Thermal and Heat Flow

Heat flow during welding can strongly affect phase transformations during welding and thus the resultant microstructure and properties of the weld. It is also responsible for weld residual stresses and distortion [14].

1.2.1.1 Heat Source Efficiency

Heat source efficiency is defined as

$$\eta = \frac{Q}{Q_{nominal}} = \frac{Q}{EI} \quad 1. 1$$

Where Q is the rate of heat transfer from the heat source to the workpiece, $Q_{nominal}$ the nominal power of the heat source, E is the constant voltage, and I constant current in the arc welding [14]. It should be noted that the term heat input often refers to $Q_{nominal}$, or EI in the case of arc welding, and the term heat input per unit length of weld often refers to the ratio $Q_{nominal}/V$, or EI/V , where V is the welding speed. Exhibit 1.6 show the heat source efficiencies measured in different welding processes.

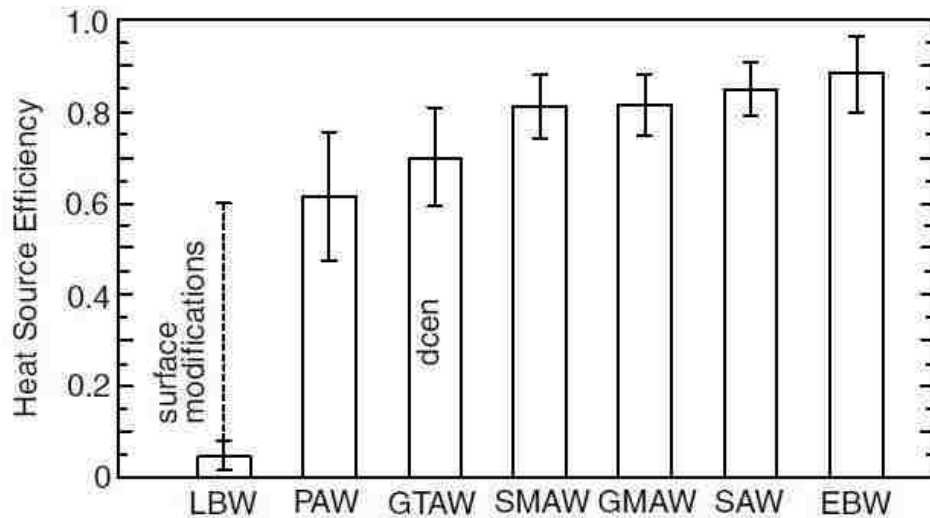


Exhibit 1-6 Heat source efficiencies in different welding methods. Reprinted from Kou [14]

1.2.1.2 Melting Efficiency

The ability of the heat source to melt the filler and the base metal is another effect of welding that should be considered. Sindo Kou represented Equation 1.2 [14] for the *melting efficiency* of the welding as follows

$$\eta_m = \frac{(A_{base} V t_{weld}) H_{base} + (A_{filler} V t_{weld}) H_{filler}}{\eta EI t_{weld}} \quad 1. 2$$

Where η_m is the melting efficiency, A_{base} is base metal contributed area, A_{filler} is the filler metal contributed area, H_{base} is the energy required to raise a unit volume of base metal

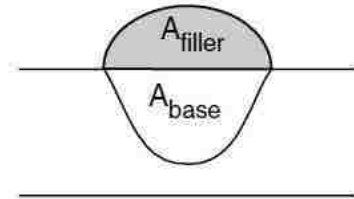


Exhibit 1-7 Cross section of welding showing areas representing contributions from base metal and filler metal [14]

to the melting point, and H_{filler} the energy required to raise a unit volume of filler metal to the melting point. The quantity inside the parentheses represents the melted material, while the denominator represents the heat transfer from the heat source to the workpiece. Exhibit 1-8a and b show the transverse cross section of two steel welds differing in the melting efficiency. Here, $EI = 3825W$ and $V = 10mm/s$ for the shallower weld of lower melting efficiency (Exhibit 1.8a) and $EI = 10170W$ and $V = 26mm/s$ for the deeper weld of higher melting efficiency (Exhibit 1.8b). Note that the ratio EI/V is equivalent in each case [14].

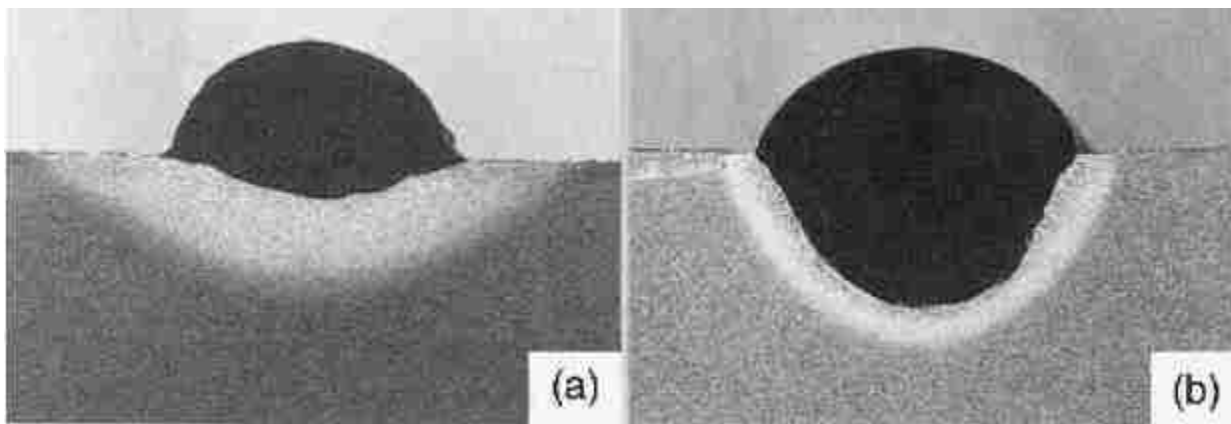


Exhibit 1-8 Melting efficiency: (a) lower at lower heat input and welding speed; (b) higher at higher heat input and welding speed [14]

Hence, Sindo Kou proposed Equations 1.3 and 1.4 for calculating melting efficiency.

$$\eta_m = A \exp\left(-\frac{B}{\frac{\eta EIV}{H\alpha\nu}}\right) \quad 1.3$$

$$A_{filler}V t_{weld} = \pi R_{filler}^2 V_{filler} t_{weld} \quad 1.4$$

$$A_{filler} = \frac{\pi R_{filler}^2 V_{filler}}{V} \quad 1.5$$

Where in Equation 1.3 A and B are constants (0.5 and 175 respectively), $H = H_{base} + H_{filler}$, α is the thermal diffusivity, and ν is the kinematic viscosity of the weld pool. And in Equation 1.4, R_{filler} and V_{filler} are the radius and feeding speed of the filler metal, respectively. If the arc efficiency η is known, the dimensionless parameter $\eta EIV/H\alpha\nu$ is also known and melting efficiency can be determined from Equation (1.3). Eventually, A_{filler} and A_{base} can be determined from Equation (1.2). Keep this in mind that the power input must be increased along with the welding speed in order to increase the melting efficiency [14].

1.2.2 Metallurgy

1.2.2.1 Recrystallization and Grain Growth

The effect of work hardening does not exist in the fusion zone and partially in the HAZ because of melting in the fusion zone and recrystallization and grain growth in the HAZ. Thus, these strength losses should be taken into account in structural designs involving welding [14]. As a result, Fracture toughness is usually poor with coarse grains in the HAZ and the fusion zone [14].

1.2.2.2 Thermal Cycles

The loss of strength in the HAZ can be explained with the help of thermal cycles, as shown in Exhibit 1-9. The closer to the fusion boundary, the higher the peak temperature becomes and the longer the material stays above the effective recrystallization temperature, T_x . Under rapid heating during welding, the recrystallization temperature may increase because recrystallization requires diffusion and diffusion takes time. Since the strength of a work-hardened material decreases

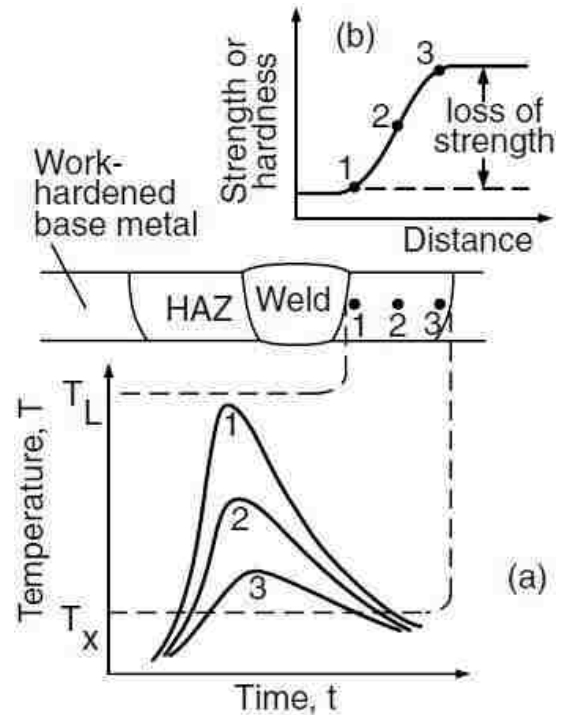


Exhibit 1-9 Softening of work-hardened material caused by welding: (a) thermal cycles; (b) strength or hardness profile Reprinted from Kou [14].

with increasing annealing temperature and time, the strength or hardness of the HAZ decreases as the fusion boundary is approached. Exhibit 1-10 shows the HAZ strength profiles of two work-hardened 5083 aluminum plates. It appears that the harder the base metal, results in the greater the strength loss [14].

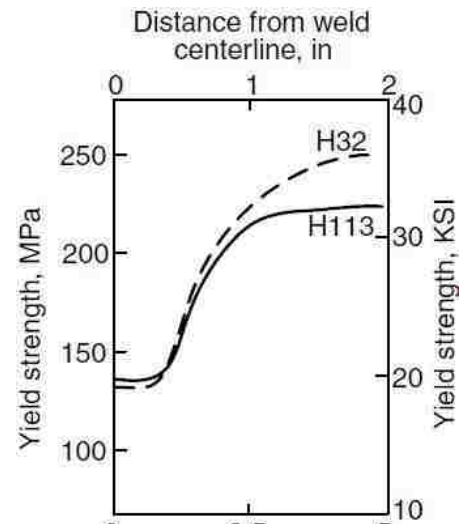


Exhibit 1-10 Yield strength profiles across welds of two work-hardened 5083 aluminum plates. Reprinted from Kou [14]

Grain growth in the HAZ can also be explained with the help of thermal cycles, as shown in Exhibit 1-11. The closer to the fusion boundary, the higher the

peak temperature becomes and the longer the material stays at high temperatures. Since grain growth increases with increasing annealing temperature and time, the grain size in the HAZ increases as the fusion boundary is approached [14].

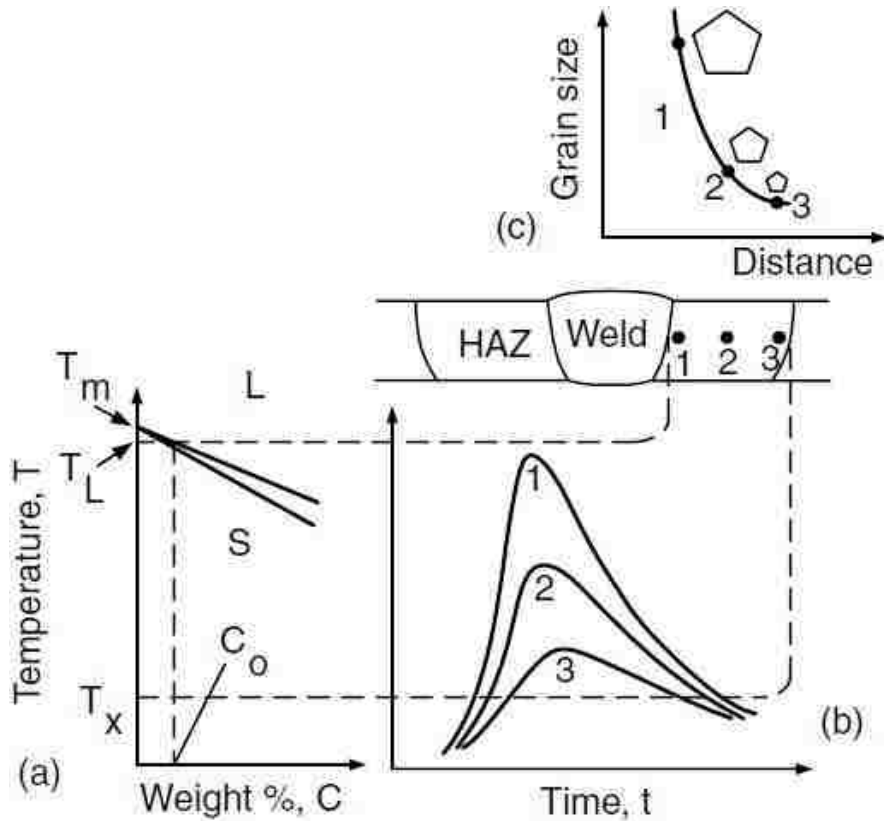


Exhibit 1-11 Grain growth in HAZ: (a) Phase diagram; (b) Thermal cycles; (c) Grain size variations. Reprinted from Kou [14]

1.2.2.3 Effect of Welding Parameters

The effect of welding parameters on the HAZ strength is explained in Exhibit 1.12. Both the size of the HAZ and the retention time above the effective recrystallization temperature T_x increase with increasing heat input per unit length of the weld, which is the ratio of heat input to welding speed. Consequently, the loss of strength in the HAZ becomes more severe as the heat input per unit length of the weld is increased. Exhibit 1.13 shows the effect of welding parameters on the HAZ strength of a work-hardened 5356-H321 aluminum alloy [14].

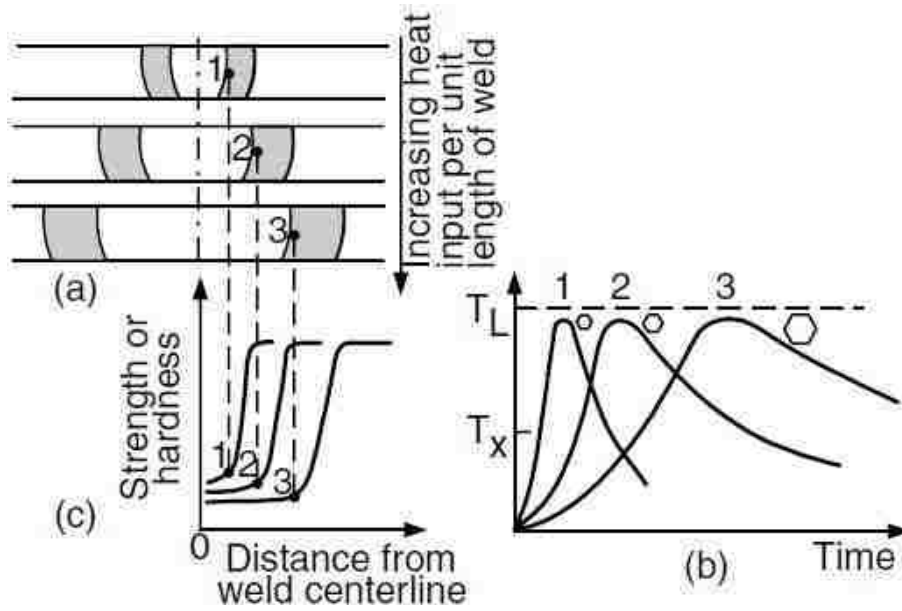


Exhibit 1-12 Effect of heat input per unit length of weld on: (a) with of HAZ (shaded); (b) Thermal cycles near fusion boundary, and (c) Strength or hardness profiles. Reprinted from Kou [14]

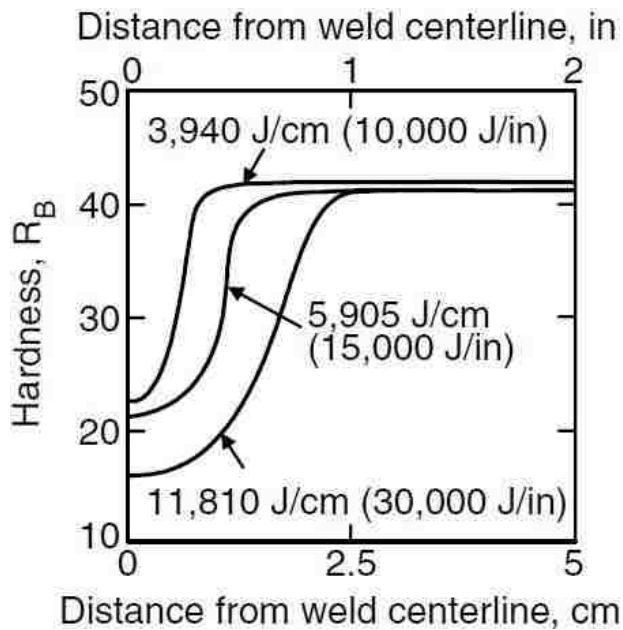


Exhibit 1-13 Effect of heat input per unit length of weld on HAZ hardness in a work-hardened 5356 aluminum. Reprinted from Kou [14]

1.2.3 Mechanical Effects

1.2.3.1 Residual Stress

Residual stresses are those stresses that will remain in a body if all external loads were removed. Welding residual stresses are one these kinds of stresses, which are a result of non-uniform temperature changes in the body. The development of residual stresses can be explained by considering heating and cooling under constraint. Three-bar arrangement is a good model for demonstrating residual stresses due to temperature changes. Exhibit 1.14 shows this demonstration.

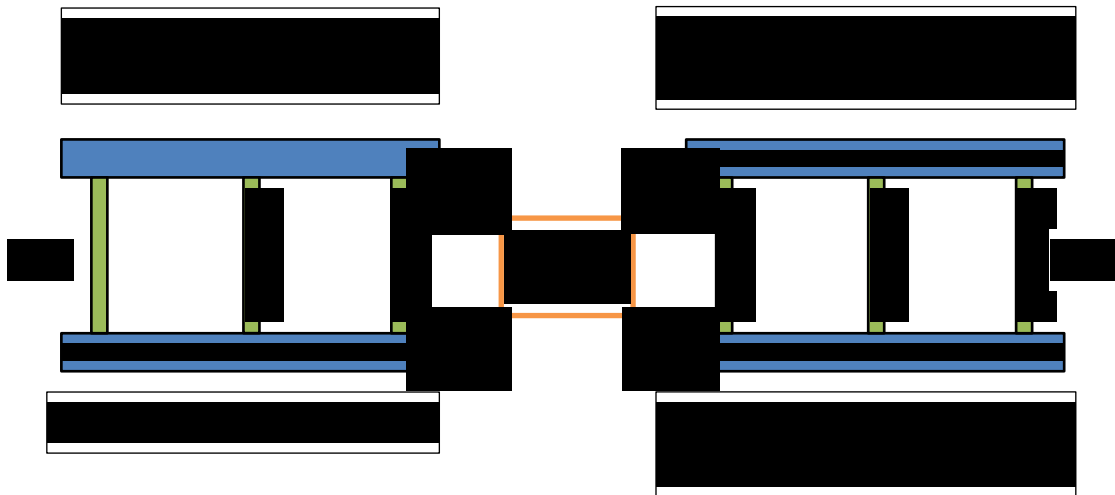


Exhibit 1-14 Demonstration of thermal residual stresses by three-bar arrangement: (a) during heating; (b) during cooling

All three bars are initially at room temperature. The middle bar alone is heated up, but its thermal expansion is restrained by the side bars (Exhibit 1.14a). Consequently, compressive stresses are produced in the middle bar, and they increase with increasing temperature until compressive stress reached the yield stress of the bar. The yield stress is the upper limit of stresses in a material, since then plastic deformation occurs. By stopping the heating and starting

the cooling phase of the middle bar, its thermal contraction is restrained by the side bars (Exhibit 1.14b). Subsequently, the compressive stresses in the middle bar drop rapidly, change to tensile stresses, and increase with decreasing temperature until the yield stress in tension is reached. Therefore, a residual tensile stress equal to the yield stress at room temperature is established in the middle bar when it cools down to room temperature. The residual stresses in the side bars are compressive stresses and equal to one-half of the tensile stress in the middle bar [14].

The three-bar demonstration is roughly presenting that how the residual stresses formed in weldments during welding process. The weld metal and the adjacent base metal are analogous to the middle bar, and the areas farther away from the weld metal are analogous to the two side bars. Exhibit 1.15 shows these residual stresses in butt weld.

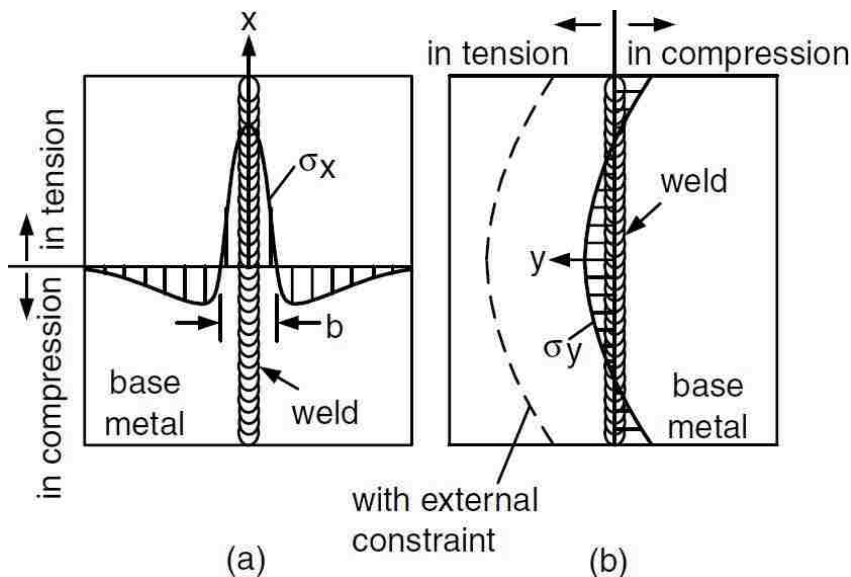


Exhibit 1-15 Typical distribution of longitudinal (σ_x) and transverse (σ_y) residual stresses in but weld. Reprinted from Kou [14]

1.2.3.2 Distortion

Due to solidification shrinkage and thermal contraction of the weld metal during welding, the weldment has a tendency to distort. Exhibit 1.16 illustrates several type of weld distortion.

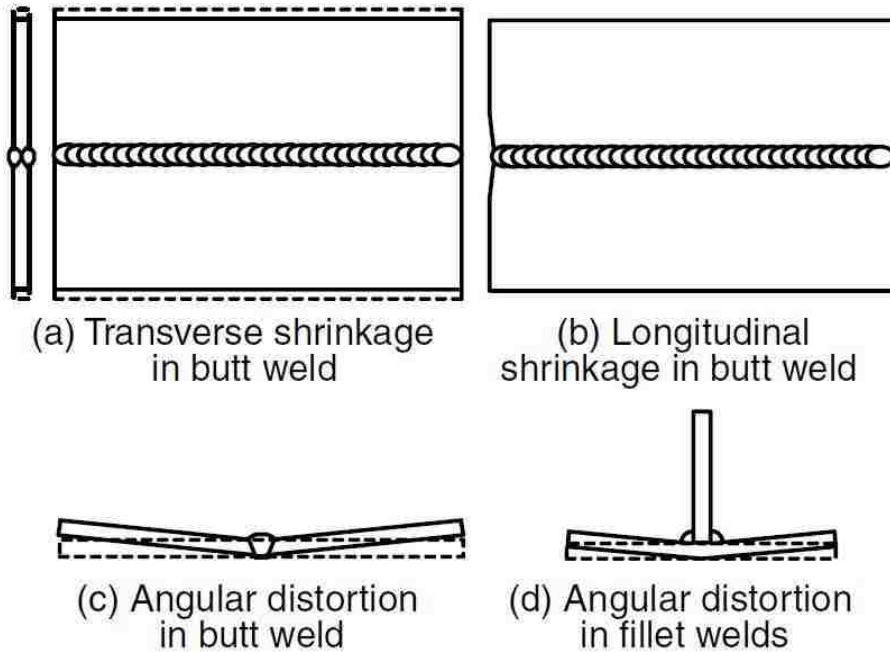


Exhibit 1-16 Typical distortion in welded parts. Reprinted from Kou [14]

1.3 Welding Simulation Process (Literature Review)

Experimental investigations usually are expensive and time consuming. Since process of arc welding is a sophisticated phenomenon, which includes heat transfer, mass transfer, element diffusion, microstructural variations, metallurgical reaction, and changes in mechanical properties, along with nonlinear geometry makes the numerical analysis very difficult to get solution. Nowadays, with powerful computers, which are equipped with 64bits high speed multicore CPUs, it is possible to simulate an accurate model of welding process.

There is several commercial finite elements software available such as ANSYS, ABAQUS, COSMOS, SYSWELD, and ALGOR, which can be used to simulate welding process.

This investigation focuses on the simulation of welding-induced residual stresses in a stainless steel pipe using ESI Visual-Weld and SYSWELD. This paper compares generated residual stresses during a single pass arc welding in axisymmetric 2-D, 3-D Shell, and full 3-D models.

Many investigations on welding residual stresses due to circumferential girth welding of pipes already have been performed. Brickstad and Josefson [4] performed a parametric study of finding residual stresses by numerical simulation of multi-pass circumferential butt-welding of stainless steel pipes and their sensitivity to variation in weld parameters. Predicted residual stresses were compared to ASME XI and then recommendations were. They simplified the problem by assuming rotational symmetry and thereby neglecting effects of heat flow in the circumferential direction ahead of the moving heat source during welding. Deng et al [15] investigated welding residual stresses in 2.25Cr-1Mo steel pipe. They developed thermal elastic plastic finite element analysis based on ABAQUS code to predict residual stress field due to the weld. Another investigation has been done by Naeem Ullah Dar et al [16] on the analysis of weld induced residual stresses and distortion in thin-walled cylinders. In order to calculate distortion and residual stresses, they employed a three-dimensional finite element model for simulation of gas tungsten arc welding (GTAW) in thin-walled pipe. The geometry of their model is based on Butt-weld with single “V” for a pipe with 300 mm outer diameter and 3mm wall thickness. And then, they validated their computational results by comparing them with the experimental measurements over temperature distribution, residual stresses, and distortion.

2 Welding Simulation

At early numerical predictions of residual stresses were essentially one-dimensional, although the analytic solution for the temperatures was two-dimensional [12]. The earliest two-dimensional finite element analysis performed in the early 1970s [12]. The reality of welding phenomena, however, is three-dimensional and transient. The first full 3-D analysis of welds was presented in 1986 [12].

In the following of this section, analytical model of temperature fields of arc welding is presented. Then the heat source modeling of arc welding is illustrated. And finally, material modeling of base metal and filler metal are discussed.

2.1 Heat Transfer Modeling of Arc Welding

The nature of arc welding is non-linear thermo-mechanical phenomena. The moving heat source results in heat generation and large thermal gradients and non-uniform temperature distribution in the workpiece all result in thermal stresses and distortions. During welding, radiation, convection, and conduction are considered as the main factors of heat transfer modeling. SYSWELD internally uses numerical method to compute heat transfer rate including radiation, convection, and conduction. Based on the conservation of energy principle, the rate of increase internal and kinetic energy for a particle equals the work done on the material plus heat input through conduction across its boundary surface and heat supply throughout its volume, that is

$$\frac{D}{Dt}(U + KE) = P + Q_c + Q_s \quad 2.1$$

Where (D/Dt) is material derivative, U denotes the internal energy of a differential volume dV at position (x, y, z) at time t , KE its Kinetic energy, Q_c the net rate of heat inflow by conduction from its surroundings, Q_s the heat supply (rate of heat input due, e.g., radiation), and P the rate of work done on the particle by body forces (in absence of body forces this assume to be equal zero) [17].

Since,

$$P = \frac{D}{Dt}(KE) + T_{ij} \frac{\partial v_i}{\partial x_j} = 0 \quad 2.2$$

$$Q_c = -\frac{\partial q_i}{\partial x_i} dV \quad 2.3$$

Hence, equation 2.1 becomes

$$\rho \frac{Du}{Dt} = -div \mathbf{q} + \rho q_s \quad 2.4$$

Where ρ is density, Du/Dt is the specific heat C_p , q_s is heat supply per unit mass, $\mathbf{q} = -\kappa \cdot \nabla T$, in which $\kappa(T)$ is the thermal conductivity, and T is the temperature. Hence by substituting Fourier's law definition in Equation 2.4 obtains

$$\rho C_p = div (\kappa \cdot \nabla T) + \rho q_s \quad 2.5$$

This is the governing equation of calculating heat transfer in welding. The product $\rho \cdot C_p$ reflects the capacity of the material to store energy.

SYSWELD prepared numerical solution for welding, which is included heat transfer, phase transformation, and linear plasticity and all are time dependent.

The boundary conditions of heat transfer in SYSWELD for an arbitrary fixed volume Ω defined as follows [13]

- Imposed temperature

$$T = T_0 \text{ at } t = 0$$

$$T_s = T_i(x, y, z, t) \text{ on surface}$$

- Heat flux density imposed on the side wall of the part

$$\kappa \cdot \nabla T \cdot \mathbf{n} = q(T, t) \text{ on surface}$$

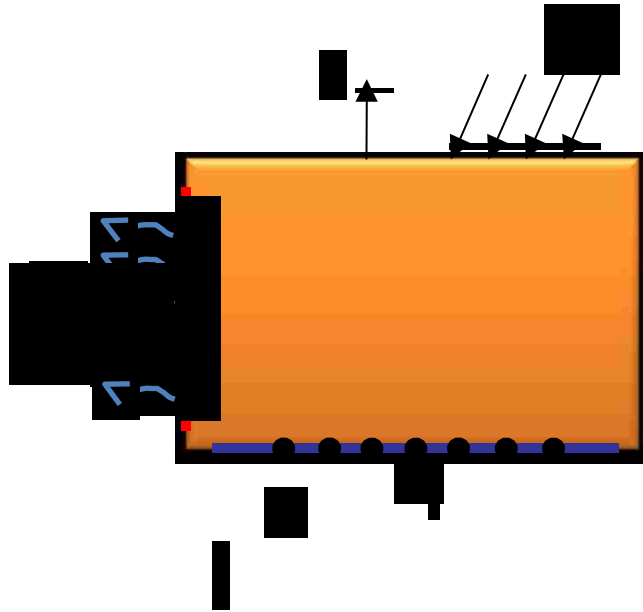
- Imposed coefficient of heat exchange

- By convection

$$q_i n_i = h(T - T_0) \text{ on surface}$$

- By Radiation

$$q_i n_i = \sigma \epsilon T^4 - \alpha q_r \text{ on surface}$$



Where h is the convection coefficient; T is unknown surface temperature; T_i is a convective exchange temperature; σ is the Stefan-Boltzmann constant; ϵ is the surface emission coefficient; α is the surface absorption coefficient, and q_r is the incident radiant heat flow per unit surface area.

2.2 Heat Source Modeling

Goldak et al. [12, 18] initially introduced a semi-ellipsoidal heat source in which heat density is distributed in a Gaussian manner. The heat density $q(x, y, z, t)$ in a moving coordination along the weld line (z-direction) is given by the following equation:

$$q(x, y, z, t) = \frac{6\sqrt{3}Q}{abc \pi\sqrt{\pi}} e^{-3\left(\frac{x^2}{a^2} + \frac{y^2}{b^2} + \frac{[z+v(\tau-t)]^2}{c^2}\right)} \quad 2.6$$

Where,

$Q = \eta UI$, is the energy input rate (power)

$\eta = \text{Heat source efficiency}$

$U = \text{voltage}$

$I = \text{current,}$

and $\xi = z + v(\tau - t)$ is the transforming relation of the fixed (x, y, z) and the moving coordinate system (x, y, ξ) ; v is the welding speed, and τ is a lag factor defined for position of the source at time $t = 0$.

Calculation and Investigation over the single heat source indicated that the predicted temperature gradient in front of the heat source was not steep enough as expected and equally, the rear gradient of the molten pool was steeper than experimental measurements. To overcome this limitation, two ellipsoidal sources were combined as shown in Exhibit 2-1. The front half of the source is the quadrant of one ellipsoidal source, and the rear half is the quadrant of another ellipsoid. The power density distribution along the ξ axis is shown in Exhibit 2-1.

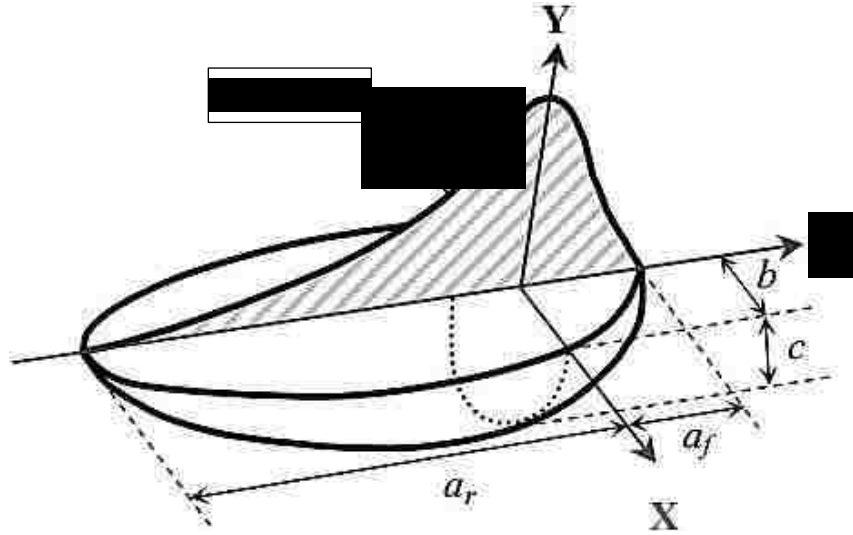


Exhibit 2-1 Goldak's Double ellipsoidal Model of arc welding heat source

For

the new model, the power density distribution inside the front and the rear quadrant respectively are:

$$q(x, y, z, t) = \frac{6\sqrt{3}f_f Q}{abc \pi\sqrt{\pi}} e^{-3\left(\frac{x^2+y^2}{a^2+b^2} + \frac{[z+v(\tau-t)]^2}{c^2}\right)} \quad 2.7$$

$$q(x, y, z, t) = \frac{6\sqrt{3}f_r Q}{abc \pi\sqrt{\pi}} e^{-3\left(\frac{x^2+y^2}{a^2+b^2} + \frac{[z+v(\tau-t)]^2}{c^2}\right)} \quad 2.8$$

Where f_f and f_r are proportional coefficient at the front and rear of the heat source, where $f_f + f_r = 2$. The parameters a, b, and c can have different values in the front and rear quadrants since they are independent.

Since the present study uses SYSWELD in order to simulate welding process, it is necessary to define the ellipsoidal heat source parameters' values for SYSWELD. The welding advisor in SYSWELD needs the information for the weld pool dimensions and energy input to complete the process of simulation. This required input includes the velocity of heat source v ,

estimated values of length, width, and penetration of weld pool, and energy input per unit length of weld that is $Q = \eta UI/v$. SYSWELD uses a script to generate the mathematical form of the heat source given by 2.7 -2.8. See Appendix A for more information about the script used in SYSWELD for defining the heat source.

3 Numerical and Computational Modeling of Circumferential Pipe Welding Using ESI Visual-Weld

Numerical simulation of the thermo–mechanical process along with progressive distribution of residual stress field during welding is highly nonlinear computational problem that requires inclusion of all the interactions between heat transfer, material transformation, and mechanical properties. A fairly complex numerical method is required to incrementally model the welding process. However, the numerical procedures can be simplified by choosing an appropriate meshed model in order to reduce the computational time. From the thermo-mechanical point of view, the heat input can be seen as a volumetric or surface energy distribution, and the fluid flow effect in the molten area can be taken into account by increasing the thermal conductivity over the fusion temperature [19].

The main goal of this study is to investigate the residual stress field and distortions arise during welding process of two stainless steel pipes. In the present study, the simulation of the arc welding will be performed by using built in explicit finite element code of SYSWELD.

In this investigation, the process of welding simulation initially begins with making the geometry of the model. Then, the FE model is developed using mesh tools in preprocessor of SYSWELD or using ESI Visual-Mesh. After defining the meshed model, the *.ASC or *.vdb file, which contains meshing data of the model, should be imported in SYSWELD or ESI Visual-

Environment. By calling Welding Advisor in SYSWELD or Visual-Environment, the material properties, geometry of the weld line, heat source parameters, and boundary conditions, has to be defined in this step. Finally, by running the solve command in SYSWELD or computation manager in ESI Visual-Environment, the process of calculation will be started.

In this section, this investigation will discuss all processes of welding simulation from creation of the geometry through post-processing and the results. The first results will illustrate the use of an axisymmetric 2-D model. This will be followed with a solid-shell model and full 3-D modeling.

3.1 Geometry and Material Properties

Simulation of the circumferential girth welding was performed on two thick-walled stainless steel pipe (316L) with an outer diameter of 120 mm, a wall thickness of 10 mm, and each has length of 250 mm as shown in Exhibit 3-1. The welding direction and the starting point of welding are also shown in Exhibit 3.2. The type of welding process modeled was general arc welding process, and single-pass welding was used to weld the pipes with a heat input of 500 J/mm and welding velocity of 15 mm/s for solid-shell and 3-D modeling. Whereas, a heat input of 35 J/mm and welding velocity of 10 mm/s are applied for axisymmetric 2-D modeling.



Exhibit 3-1 Half plane 3-D modeling of girth welding of pipe

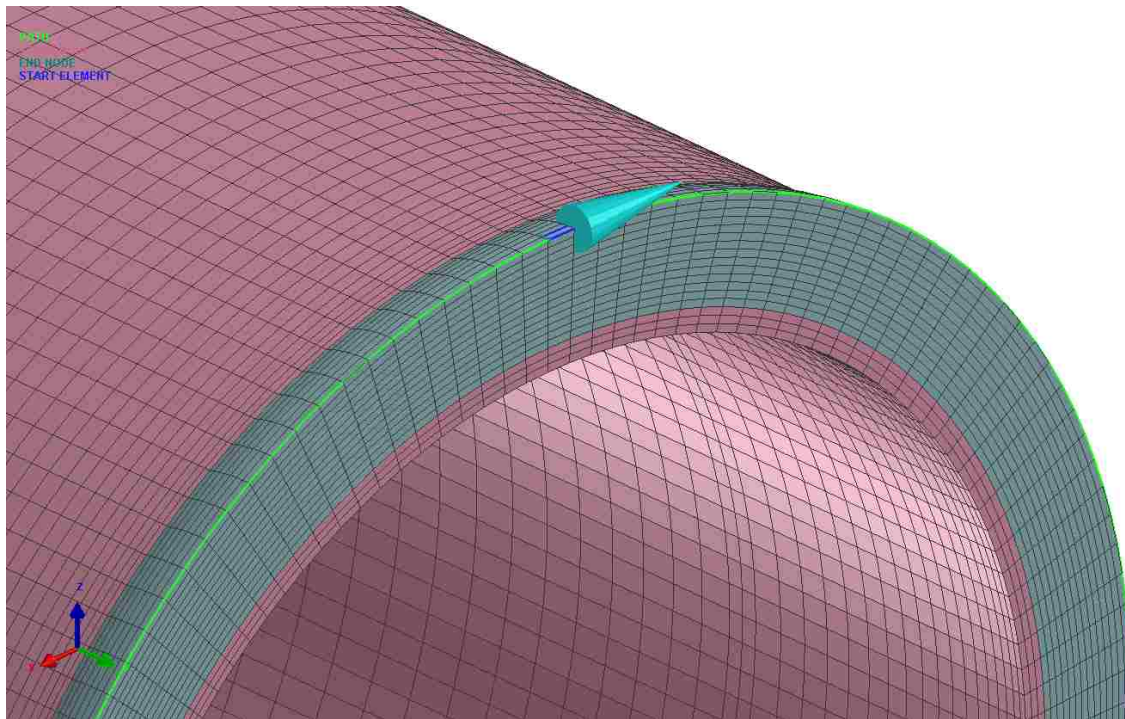


Exhibit 3-2 Welding direction and start point

The pipe as a welding component was austenitic stainless steel 316L and the filler material also is the same as the base metal. Type 316 is an austenitic chromium-nickel stainless steel containing molybdenum. This stainless steel is known for its corrosion resistance against chloride ion solutions, sulfuric, hydrochloric, acetic, and formic and tartaric acids, acid sulfates and alkaline chlorides. Type 316L is an extra-low carbon version of Type 316 that minimizes harmful carbide precipitation due to welding [20].

The common uses are exhaust manifolds, furnace parts, heat exchangers, jet engine parts, pharmaceutical and photographic equipment, chemical equipment, digesters, tanks, evaporators, pulp, paper and textile processing equipment, parts exposed to marine atmospheres and tubing. 316L is used widely as welding components due to its resistance against carbide precipitation during welding process results in more assuring optimum corrosion resistance.

The chemical compositions and mechanical properties are specified in Table 3-1 and Table 3-2.

Carbon	Manganese	Phosphorus	Sulfur	Silicon	Chromium	Nickel	Molybdenum	Nitrogen	Iron
0.03	2.00	0.045	0.03	0.75	16-18	10-14	2-3	0.1 max	Balance

Table 3-1 Chemical composition of stainless steel 316L

UTS (MPa)	0.2% Yield Strength (MPa)	% Elongation in 2" (50.8 mm)	Hardness Rockwell
558	290	50	B79

Table 3-2 Mechanical properties at room temperature

3.2 Axisymmetric 2-D Modeling of Pipe Girth Welding

Since 3-D finite element model of pipe welding needs a long computational time, a 2-D axisymmetric model is an alternative method to simplify the problem by assuming that the

welding speed is sufficiently fast relative to the heat conduction rate of the welded metal [15], thus permitting neglect of circumferential heat transfer effects. This investigation used axisymmetric rotational modeling in ESI Visual-Weld in order to simulate welding process and then finding residual stresses.

3.2.1 Geometry of the Welded Components

The geometry of the 2-D axisymmetric model of the pipe components and the weld were initially created in AutoCAD, then, it exported as a *.IGES file, and then imported into Visual-Mesh in order to create the meshed model. In this study, the axisymmetric model was developed using quadratic meshing elements. Exhibit 3-3 shows the geometry of axisymmetric model of pipe girth welding.

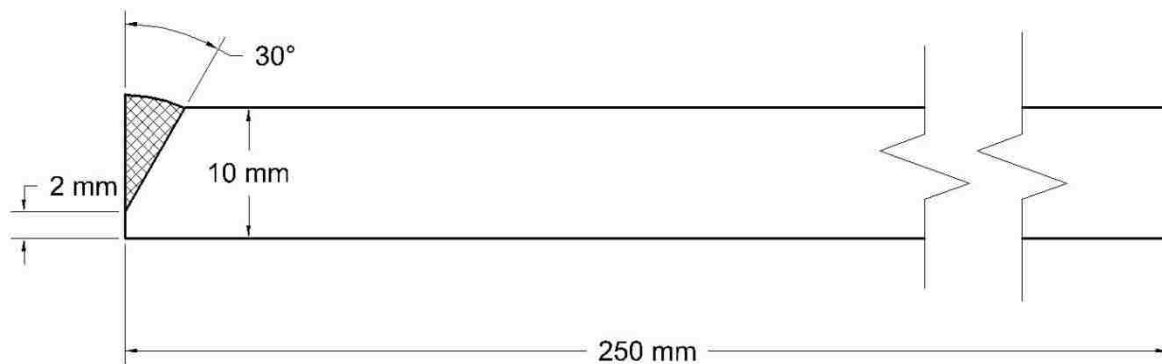


Exhibit 3-3 Geometry of Axisymmetric 2-D model of Pipe Welding

3.2.2 Axisymmetric Meshed Model

Exhibit 3-4 shows the meshed axisymmetric 2-D model. For making meshes, ESI Visual-Mesh was used to make the meshed model. The meshed model in this case contained 1342 nodes and 1449 elements.

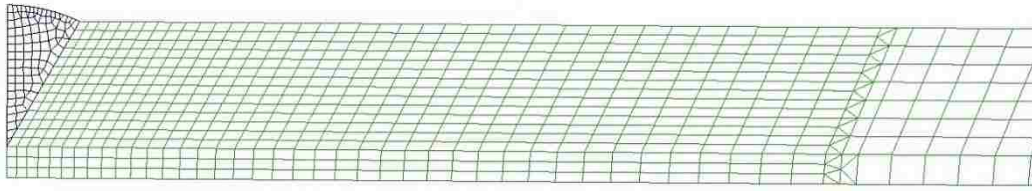


Exhibit 3-4 Meshed axisymmetric 2-D model of a welded pipe

3.2.3 Boundary Conditions and Clamping

Boundary heat loss, predominantly by surface convection and radiation, affects the weld-cooling rate. The convective heat loss was modeled using the Newton's cooling law. The heat loss boundaries were assumed to be in the inner and outer surfaces of the pipe. These boundaries of the model have been extracted from 2-D open faced elements of the meshed model. The symmetric plane and clamping condition are defined as shown in Exhibit 3-5.

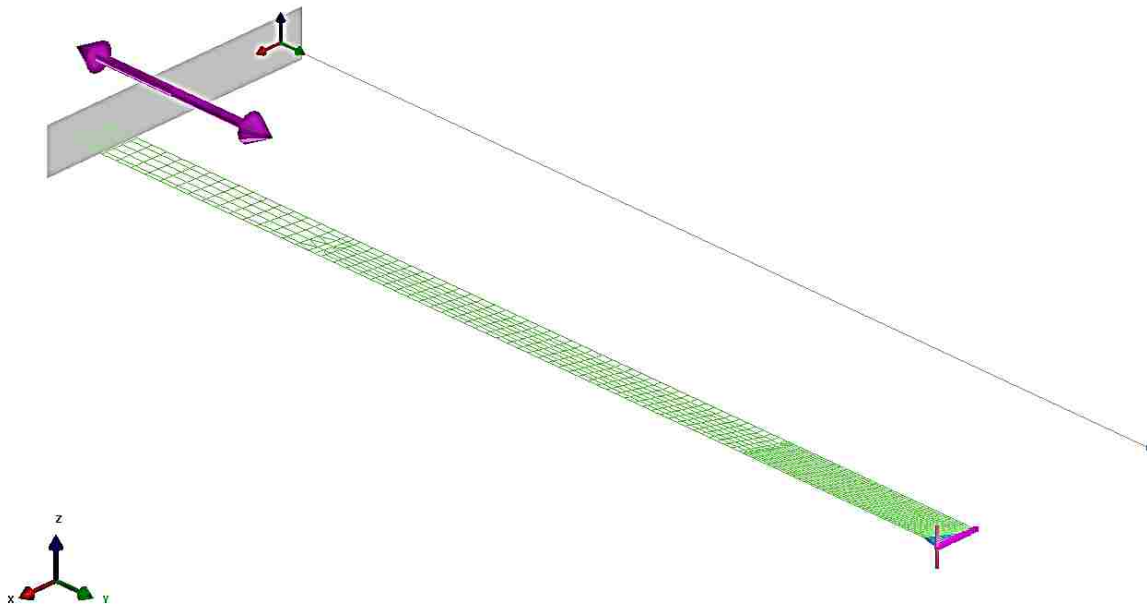


Exhibit 3-5 Clamping condition and symmetric plane of axisymmetric model

3.2.4 Thermal Analysis and Results

A heat source with a speed of 10 mm/s moves along the weld joint in the axisymmetric modeling. The total arc energy input per unit length to the joint was 35 J/mm. The energy input efficiency in this investigation supposed to be 1 since it is not a main factor to affect final results, which means the whole heat was applied to the model. The weld penetration depth is equal to 80% of wall thickness. The results of the temperature fields after running of weld simulation is shown in Exhibit 3-6, 3-7, and 3.8.

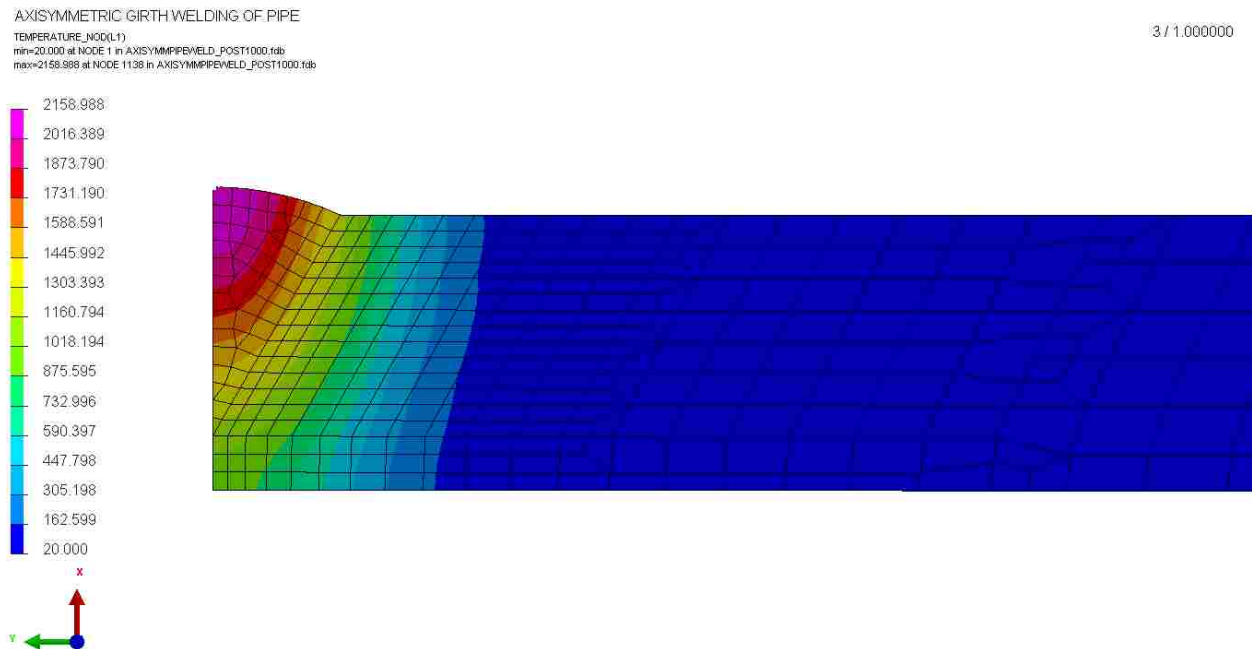


Exhibit 3-6 Temperature field after passing of the heat source °C

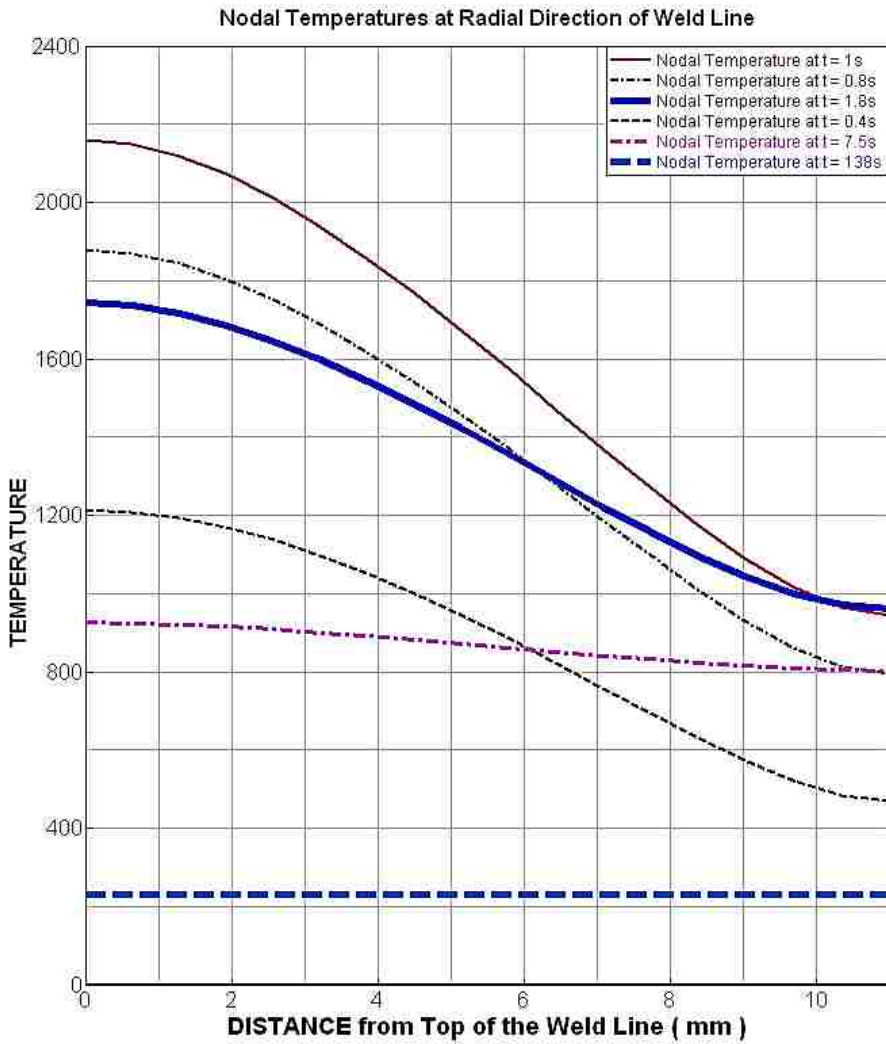


Exhibit 3-7 Nodal Temperature ($^{\circ}C$) at the center of weld line from top to bottom in different time ($t=1s$ is the passing time of heat source from the section)

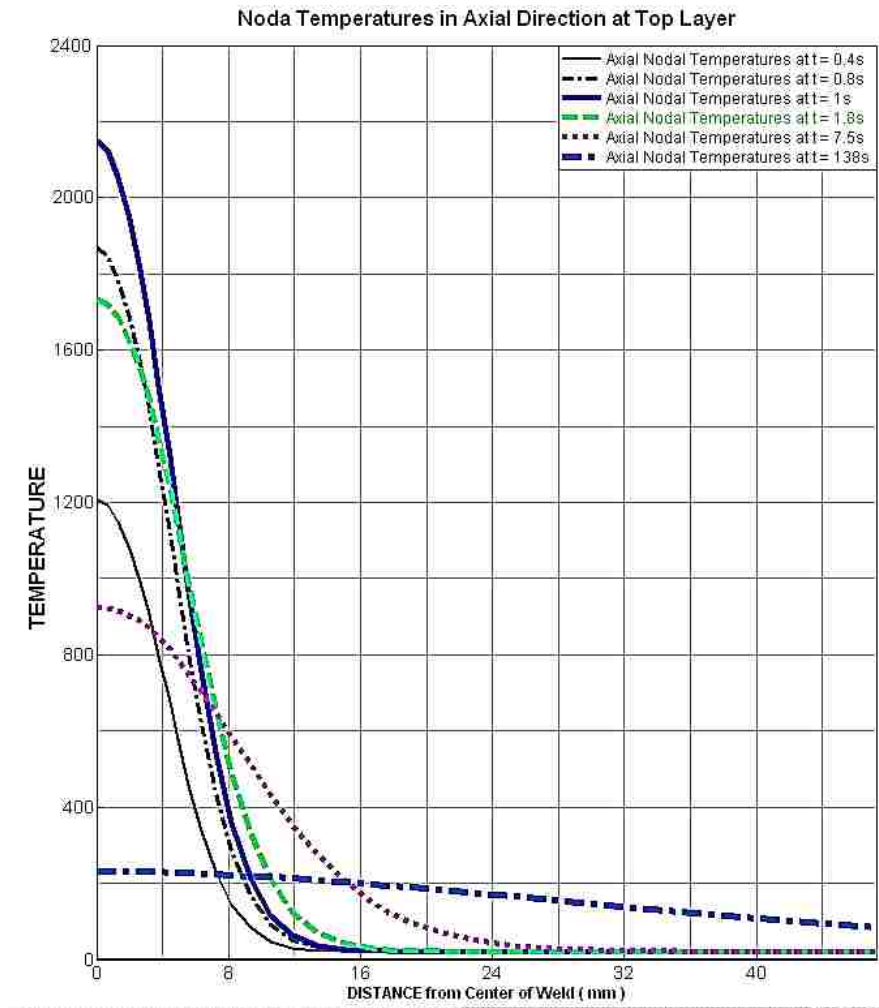


Exhibit 3-8 Nodal Temperature (°C) in axial direction at the outside surface of pipe

3.2.5 Residual Stress Analysis and Results

The residual stresses are shown in the following pictures. The axial stress, hoop stress, and von Mises stress are shown in Exhibit 3.9, 3.10, and 3.11, respectively.

AXISYMMETRIC PIPE WELDING:

STRESSES_NOD_VY(L1)
min=-355.318 at NODE 340 in AXISYMMPIPEWELDING-1_V_POST2000.tdb
max=290.518 at NODE 1957 in AXISYMMPIPEWELDING-1_V_POST2000.tdb

5 / 2000.000122

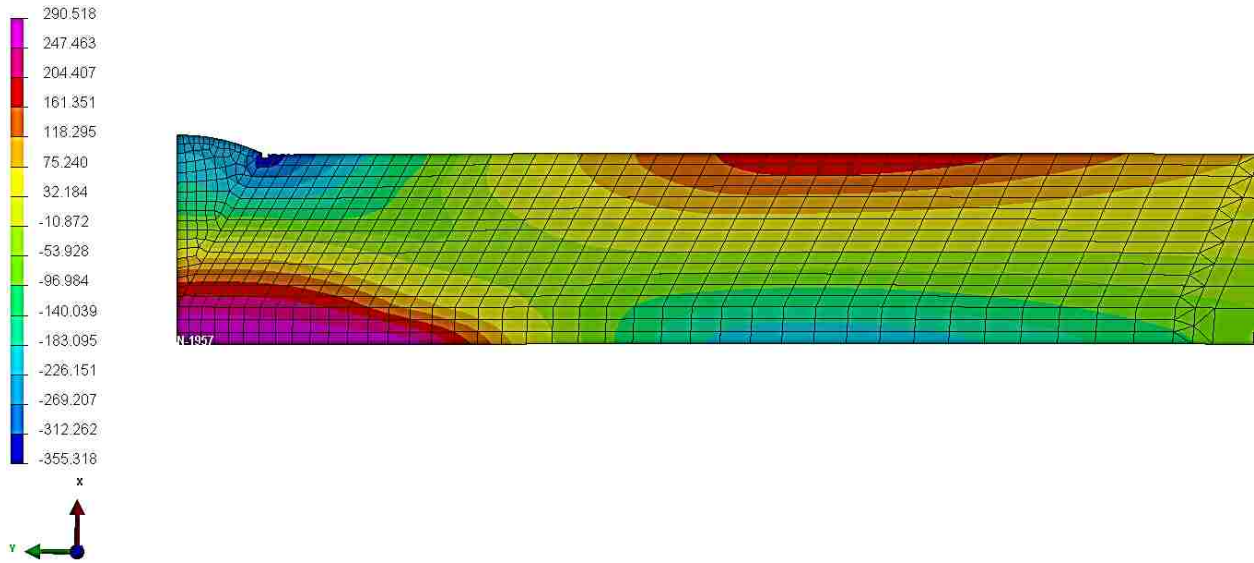


Exhibit 3-9 Axial stress field in axisymmetric modeling of pipe girth welding (MPa)

AXISYMMETRIC PIPE WELDING:

STRESSES_NOD_ZZ(L1)
min=-260.698 at NODE 1629 in AXISYMMPIPEWELDING-1_V_POST2000.tdb
max=362.589 at NODE 1451 in AXISYMMPIPEWELDING-1_V_POST2000.tdb

5 / 2000.000122

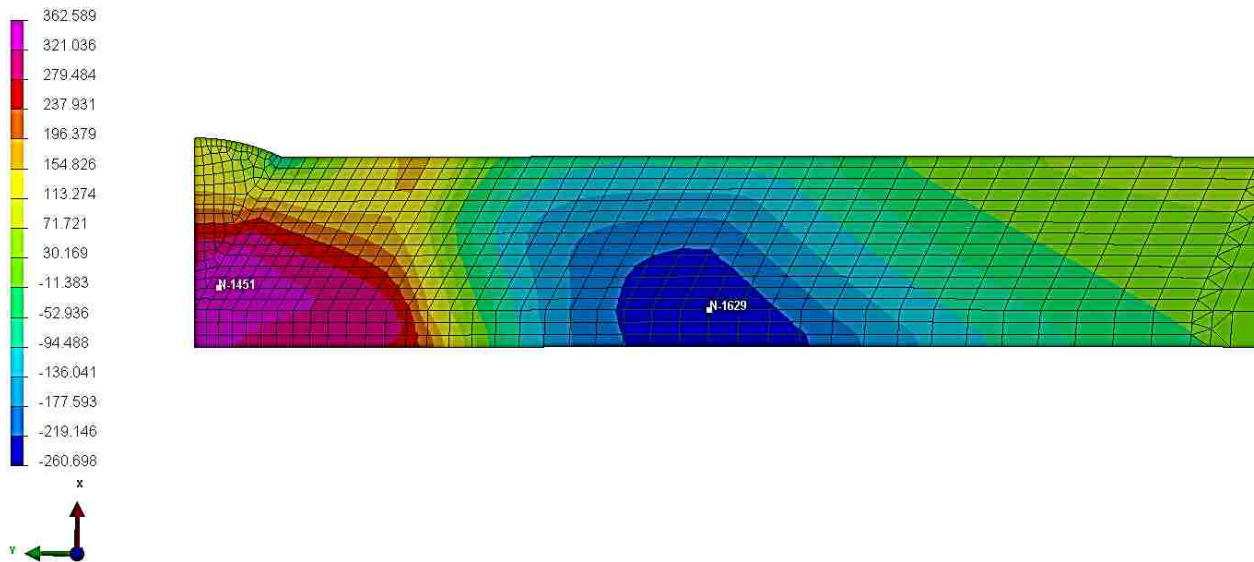


Exhibit 3-10 Hoop stress field in axisymmetric modeling of pipe girth welding (MPa)

STRESSES_NOD_Von Mises(L1)
 min=0.000 at NODE 2215 in AXISYMPPIPEWELDING-1_V_POST2000.fdb
 max=321.795 at NODE 2229 in AXISYMPPIPEWELDING-1_V_POST2000.fdb

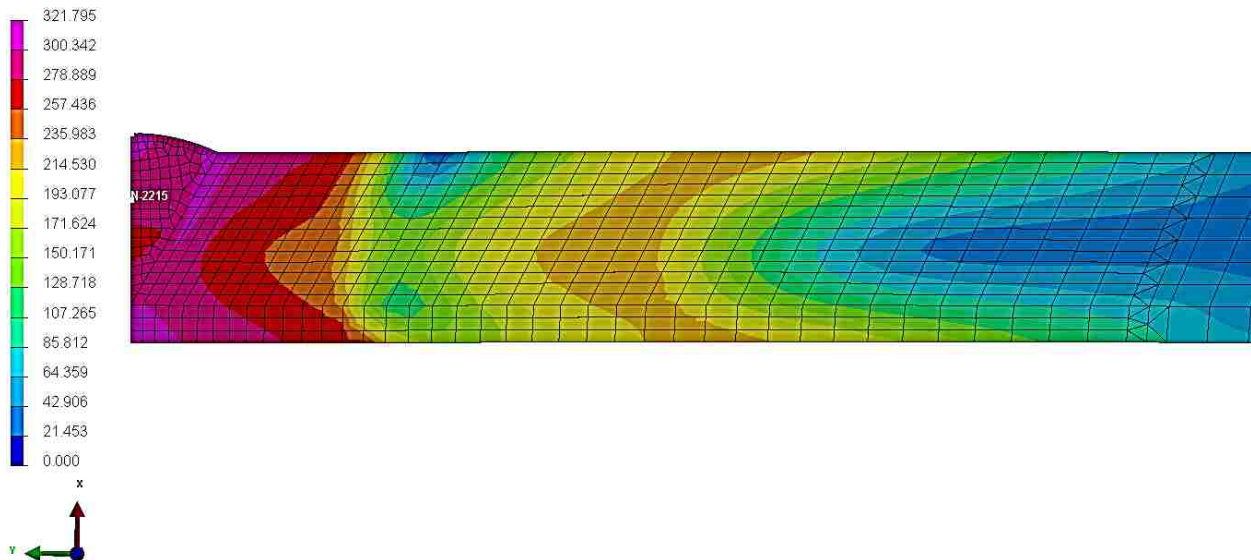


Exhibit 3-11 von Mises stress field in axisymmetric modeling of pipe girth welding (MPa)

3.3 Shell Modeling of Pipe Girth Welding

Shell models provide another method of simulation in order to reduce computational time in FE analysis. In the area of heat affected zone (HAZ), 3-D modeling is repeated. However, by using shell elements away from this region will considerably decrease the number of degree of freedoms in the welding model, resulting in reducing the computational size of 3-D modeling. There are many things that are different from standard 3-D analysis. In mechanical analysis, there are six of degrees of freedom for shell elements ($u_x, u_y, u_z, r_x, r_y, r_z$), in contrast to the three degree of freedom for three dimensional elements (u_x, u_y, u_z) [21].

The geometry of shell element modeling of pipe girth welding is the same as the 3-D modeling, but there are no 3-D elements in the thickness, i.e., all shell elements are 2-D elements with zero thickness, which this causes having much less degrees of freedom in the model. The shell model has 120 mm outer diameter with 250 mm length along with 3.85 mm width of

welding filler material deposited in the weld line. The meshed half-model and clamping condition are shown in Exhibit 3.12 and 3.12. All welding parameters are the same as 3-D modeling as given in the beginning of section 3.1.

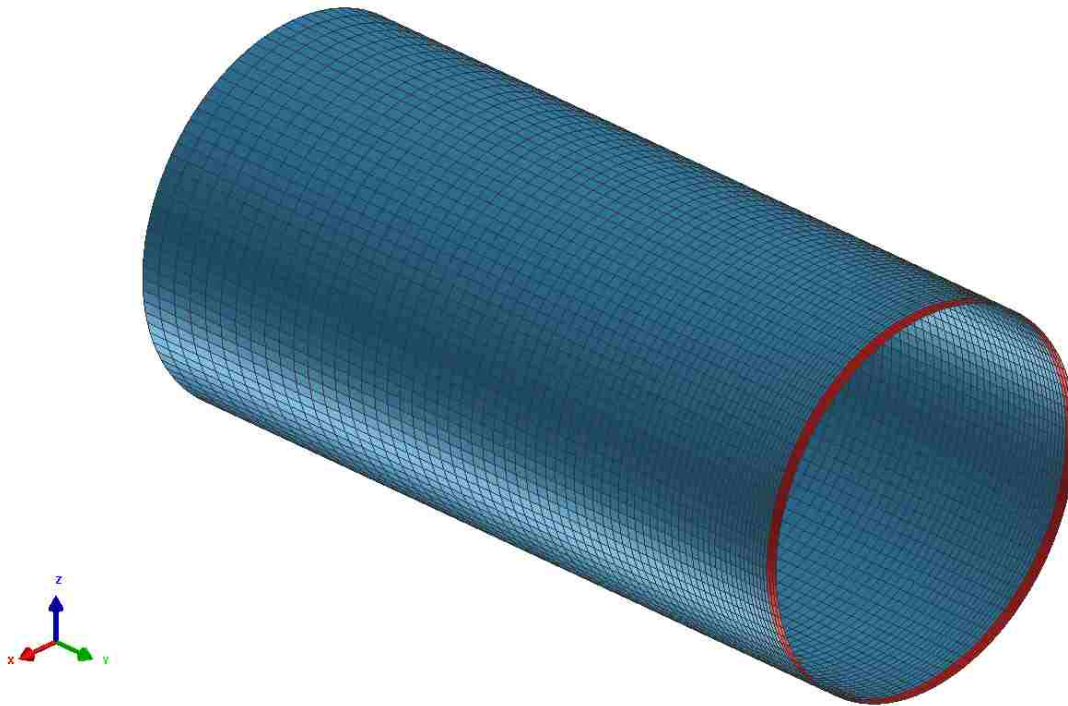


Exhibit 3-12 Shell modeling and its geometry

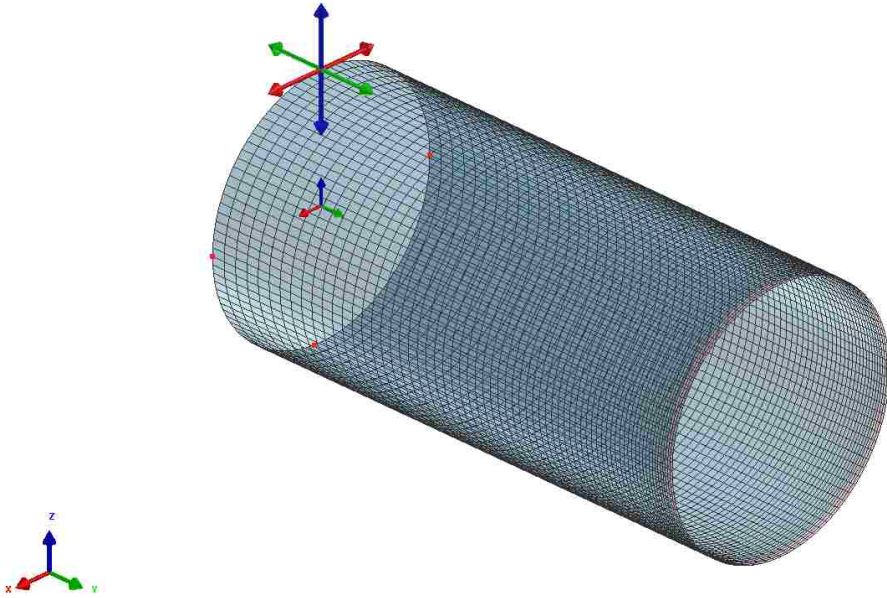


Exhibit 3-13 Clamping Condition of shell model

The clamping condition in this simulation, as shown in Exhibit 3-13, is a four points prevented from translating and rotating in all three directions between starting time and the end of welding when the heat source removed and the cooling process begins. Additionally, there is a symmetric plane defined for entire simulation process located in xz plane at the cross section of the pipe where the weld line is located.

3.3.1 Thermal Analysis and Results

Temperature contour during welding is shown in Exhibit 3.14. Temperature profile during and after welding (cooling time) is shown in exhibit 3.15.

SHELL MODELING OF CIRCUMFERENTIAL PIPE WELDING

66 / 25.522011

TEMPERATURE (NOODLTY)
min=19.990 at NODE 7200 in SHELLMODE_PPBEWELDING
max=1944.635 at NODE 7216 in SHELLMODE_PPBEWELDING

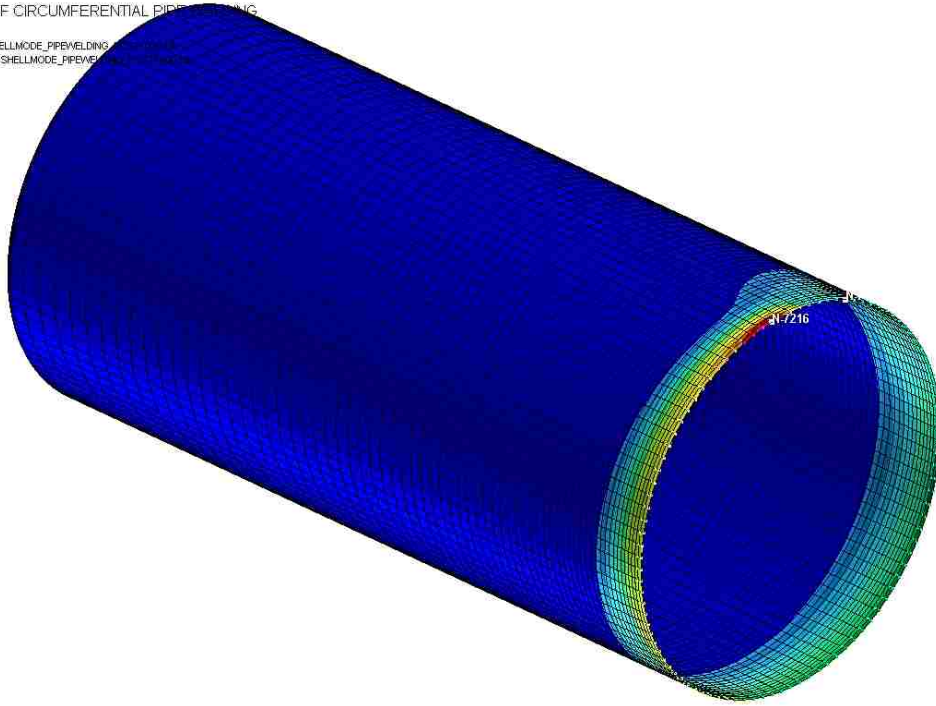
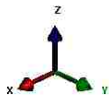


Exhibit 3-14 Temperature Contour ($^{\circ}C$) during welding at time $t = 25.5s$

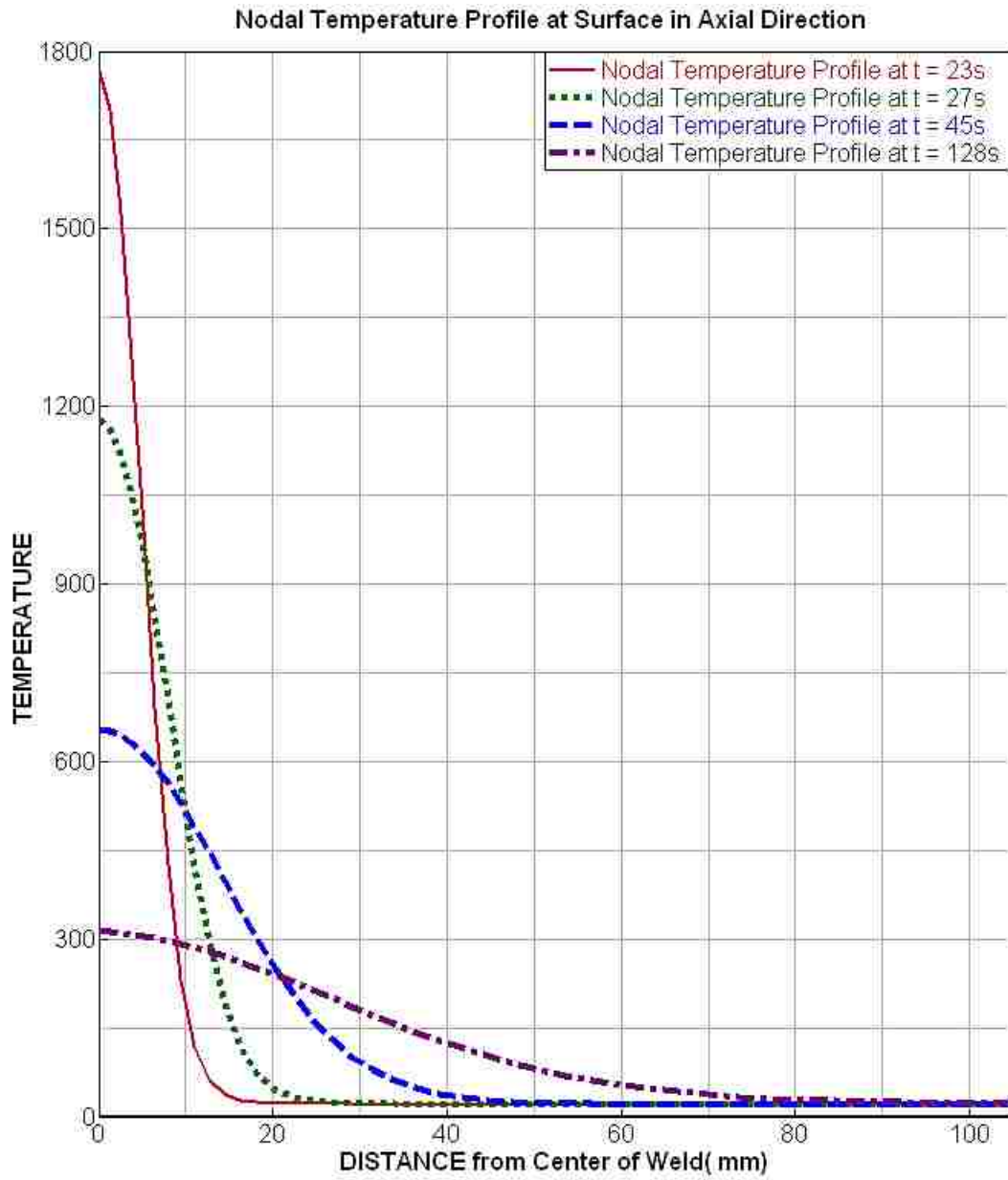


Exhibit 3-15 Nodal temperature profile (°C) at the surface of shell in axial direction

3.3.2 Residual Stress Analysis and Results

Exhibit 3-15 shows nodal axial stress contour at the surface of shell modeling of girth pipe welding.

SHELL MODELING OF CIRCUMFERENTIAL PIPE WELDING

SHELL_SURF_STRESSES_NOD_INF_VY(L1)
min=-341.938 at NODE 7226 in SHELLMODE_PIPEWELDING.L1_V1_POST23001.dat
max=228.123 at NODE 1915 in SHELLMODE_PIPEWELDING.L1_V1_POST23001.dat

5 / 2999.999756

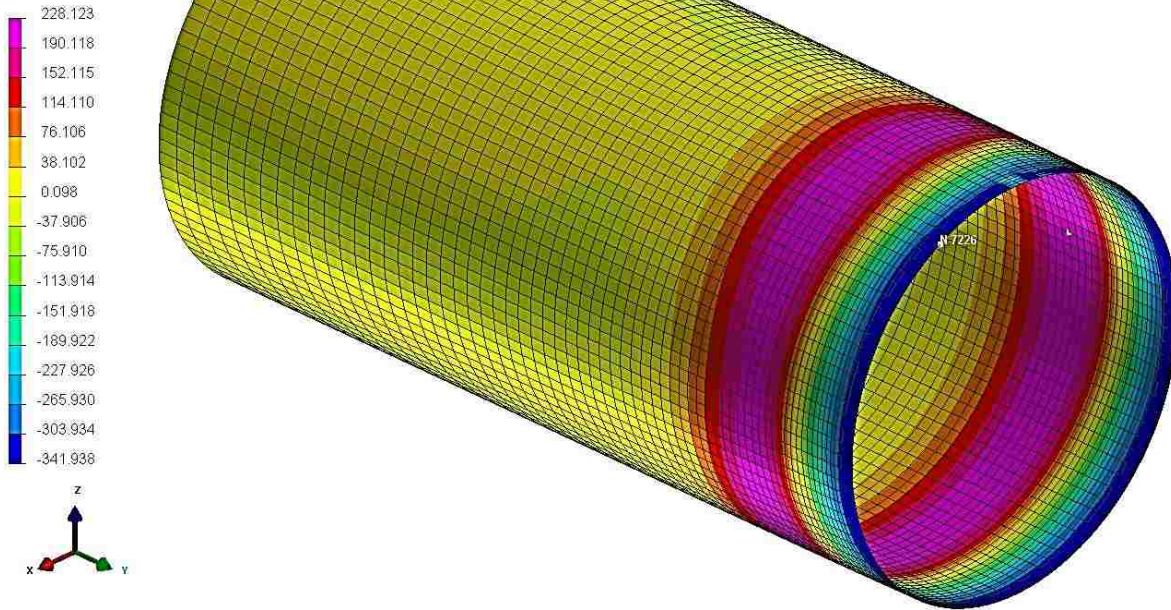


Exhibit 3-16 Axial Stress in shell modeling of pipe girth welding (MPa)

SHELL MODELING OF CIRCUMFERENTIAL PIPE WELDING

SHELL_SURF_STRESSES_NOD_INF_VX(L1)
min=-341.925 at NODE 7226 in SHELLMODE_PIPEWELDING.L1_V1_POST23001.dat
max=224.155 at NODE 1915 in SHELLMODE_PIPEWELDING.L1_V1_POST23001.dat

5 / 2999.999756

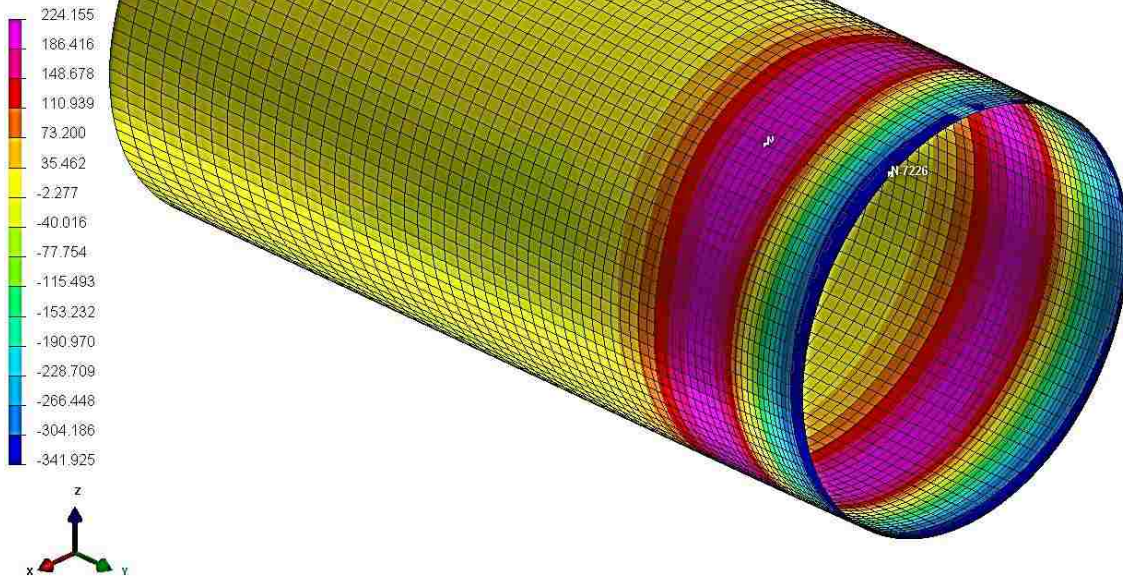


Exhibit 3-17 Hoop Stress in Cylindrical coordinate in shell modeling of pipe girth welding (MPa)

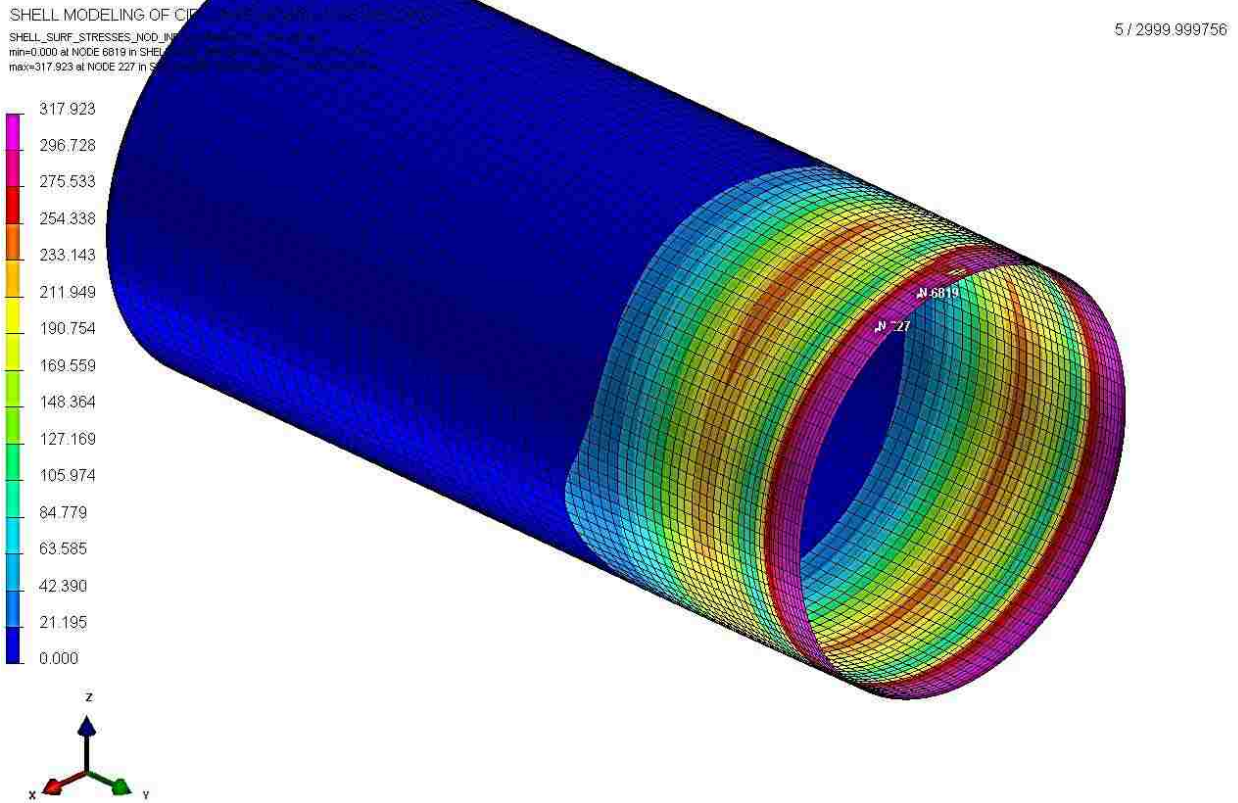


Exhibit 3-18 17 von Mises Stress distribution in shell modeling of pipe girth welding (MPa)

3.4 3-D Modeling of Circumferential Girth Welding of Pipe

Due to the nature of 3-D problems in simulation of welding process, which is complexity of the thermo-mechanical as well as phase transformation of the materials during welding in associating with degrees of freedom of nodes in three-dimensional elements, it potentially can be highly time consuming to get the results. Specifically, in the process of 3-D modeling of girth welding of pipe, the time consumption for getting the solution is highly depending on number of elements and nodes in the meshed model. It is highly important for 3-D modeling of welding simulation to apply a refined mesh in the heat affected zone area in order to get desirable solution.

In this study, a very fine meshing texture is applied to the welding area as shown in Exhibit 3-1 in the section 3. All heat source and welding parameters, explained in section 3.1, are applied to the 3-D model. The properties of meshes are specified as follows.

- 28586 2-D elements, which are mostly defined for boundary condition definitions used in air heat exchanging and clamping
- 95840 3-D elements are defined for 3-D solution known in SYSWELD as WELDGROUP and material properties applied for these 3-D elements
- 107362 nodes

The welding parameters used in this simulation assumed to be as follows:

- Welding speed – 15 mm/s
- Energy input per length – 500 J/mm (where *Voltage* $U = 30$, *Current* $I = 250$, and $v = 15\text{mm/s}$), and for the second time 975 J/mm (where *Voltage* $U = 48.75$, *Current* $I = 300$, and $v = 15\text{mm/s}$)
- Estimated length of welding pool – 15mm
- Estimated width of welding pool – 9mm
- Estimated welding pool penetration – 8mm
- Energy input efficiency – 1.00

3.4.1 Thermal analysis and results

Exhibit 3-19 shows the temperature distribution during moving of heat source along the weld line.

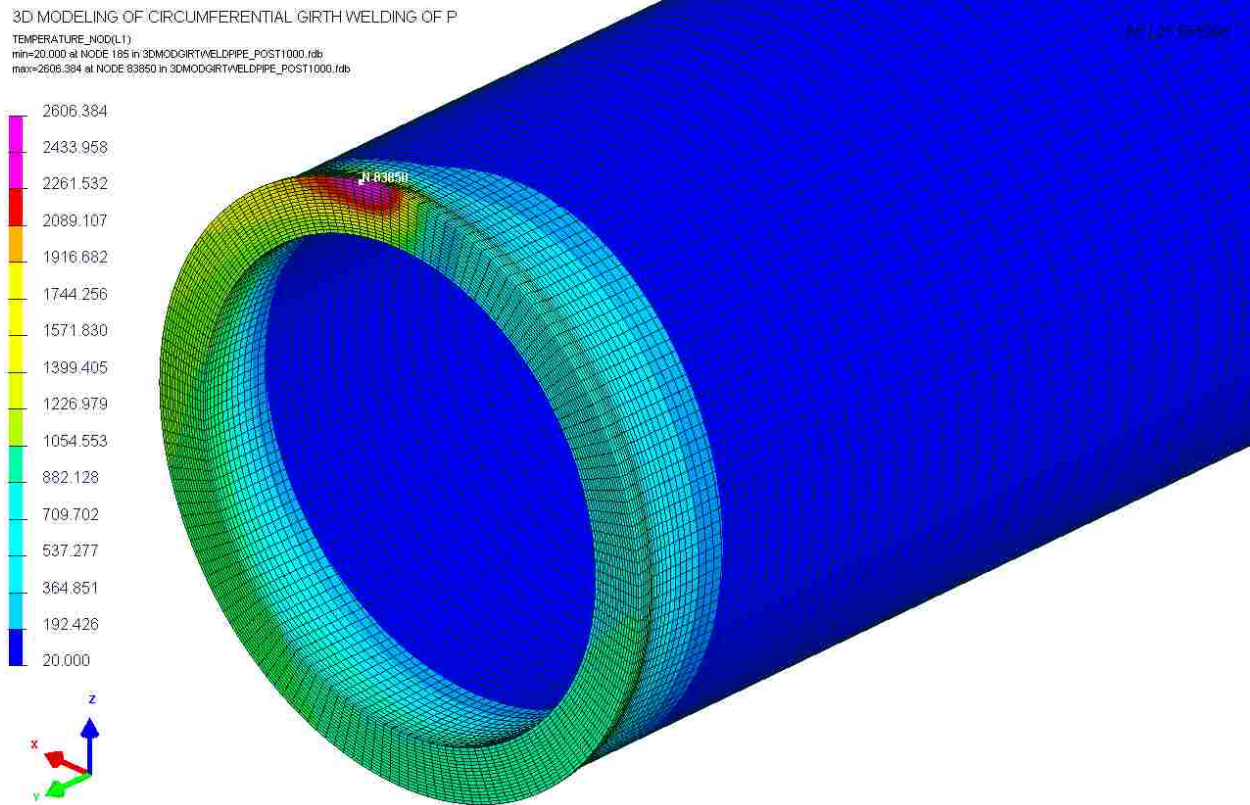


Exhibit 3-19 Temperature distribution ($^{\circ}\text{C}$) during welding at time $t = 25.5$

3.4.2 Residual Stress Analysis and Results

The axial residual stresses distribution is shown as Exhibit 3-20, and hoop residual stress distribution in cylindrical coordination is shown in Exhibit 3-21.

3D MODELING OF CIRCUMFERENTIAL GIRTH WELDING OF PIPE

STRESSES_NOD VY(L1)
min=-2.732e+002 at NODE 52826 in 3DMODGRTWELDPPE-1_V_POST2000.rdb
max=2.619e+002 at NODE 94118 in 3DMODGRTWELDPPE-1_V_POST2000.rdb

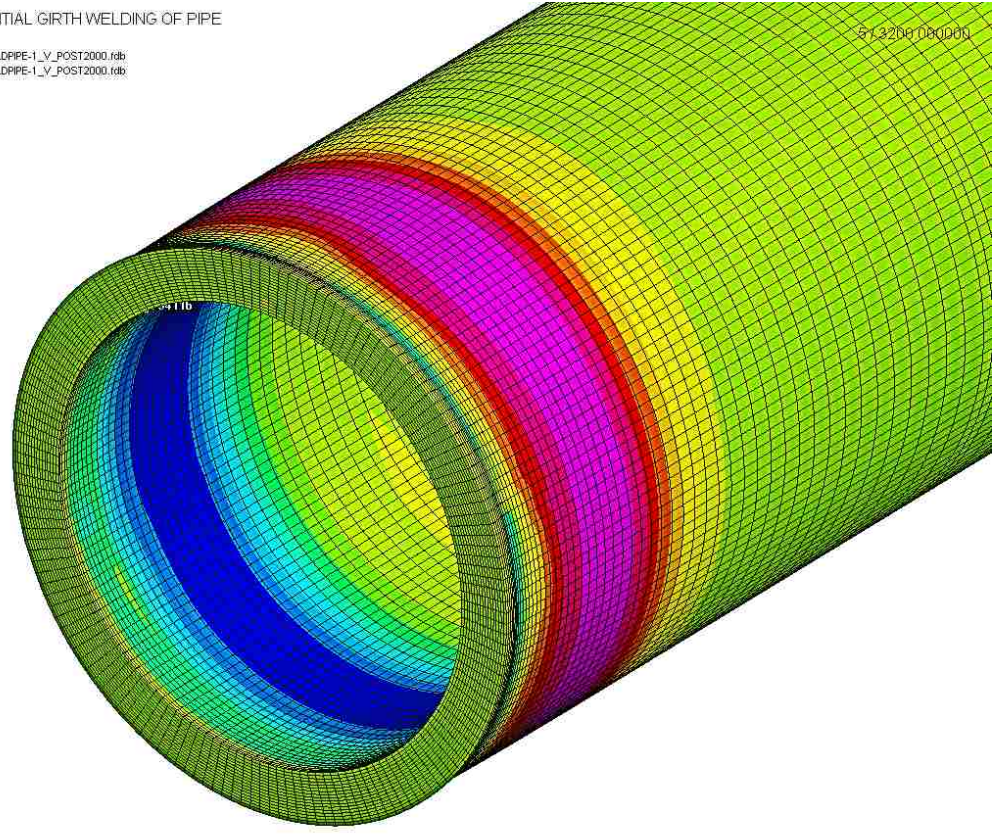
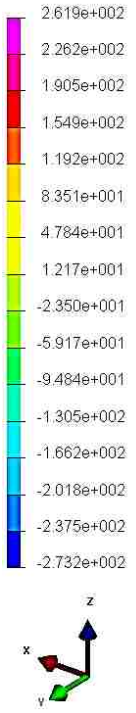


Exhibit 3-20 Distribution of Axial Stresses in 3-D simulation of girth welding of pipe (MPa)

3D MODELING OF CIRCUMFERENTIAL GIRTH WELDING OF PIPE

STRESSES_NOD XX(L1) (Cylindrical)
min=-272.297 at NODE 24644 in 3DMODGRTWELDPPE-1_V_POST2000.rdb
max=261.325 at NODE 94116 in 3DMODGRTWELDPPE-1_V_POST2000.rdb

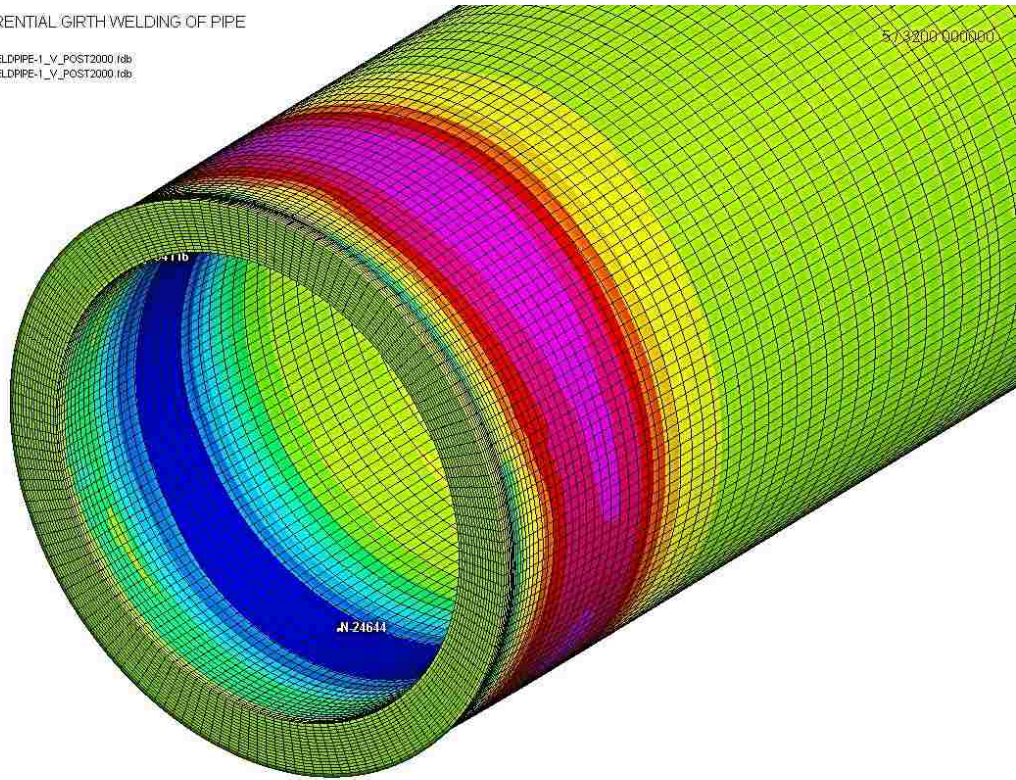


Exhibit 3-21 Hoop residual stress distribution in cylindrical coordination (MPa)

4 Final Results and Discussions

Results are next presented for the investigation of residual stresses due to welding in the stainless steel girth-welded pipe. The first step of collecting the results in this investigation is comparing the residual stresses obtained from the simulation of girth welding of pipes. The main residual stresses, which are concentrated in this study, are axial, hoop, and von Mises stresses. This study is planned to compare these stresses resulting from 2-D axisymmetric model, shell model, and half 3-D model simulation of girth welding of pipes. The comparison results of axial stresses generated at the inside and outside surface of the pipe resulting from these three methods of simulation with respect to axial distance from the weld centerline are shown in Exhibit 4-1 and 4-2. In these comparison, two different heat input applied to the 3-D model in order to compare the variation of the results due to change in this welding parameter.

Inside Surface Axial Stresses Comparison

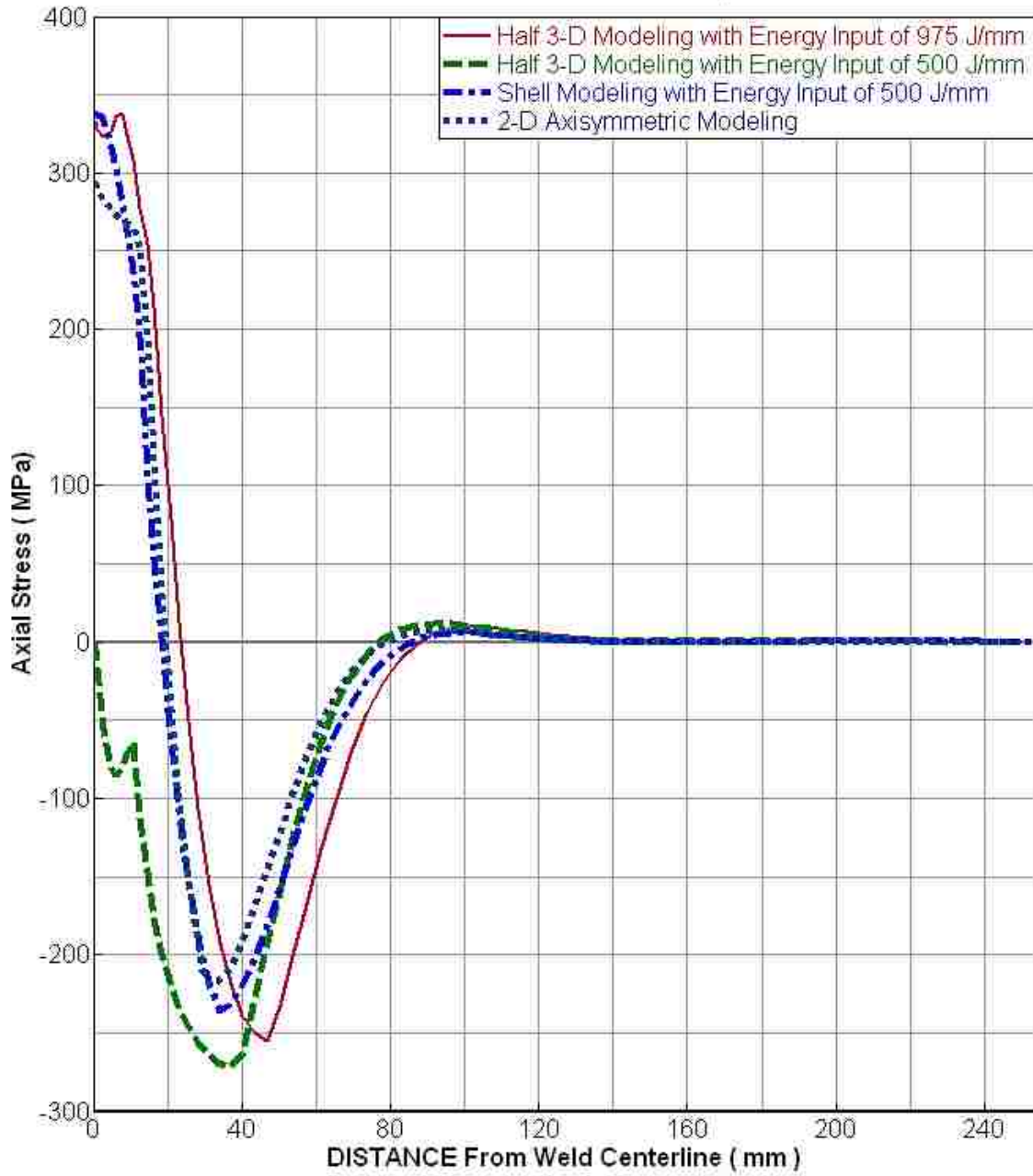


Exhibit 4-1 Comparison of axial stresses at the inside surface of the pipe

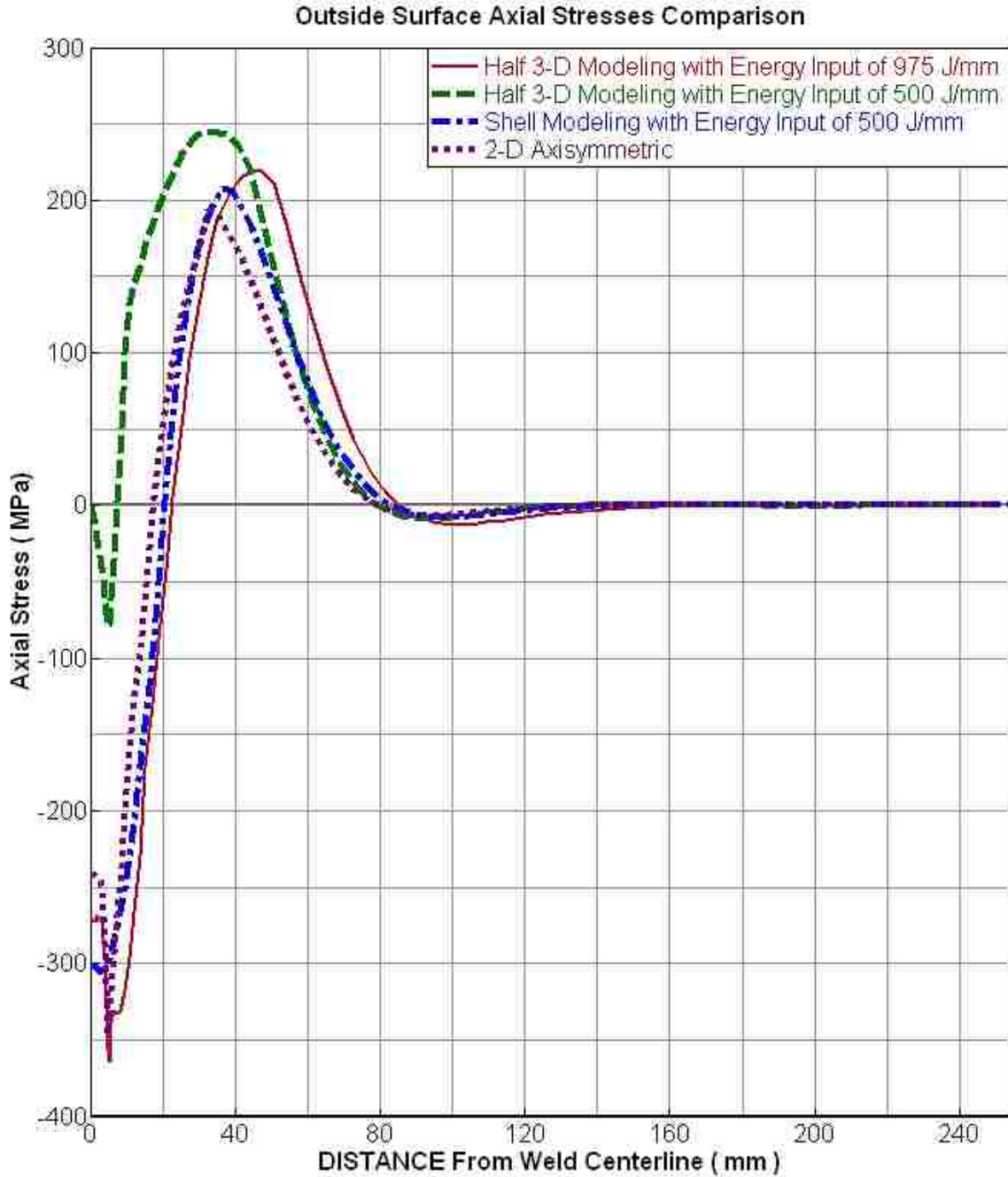


Exhibit 4-2 Comparison of axial stresses at the outside surface of the pipe

As seen in above comparison graphs, there is a perfect fitting between the shell and 2-D axisymmetric model and the 3-D model when a high-energy input applied to the 3-D model (975 J/mm, which results in high temperature in melting pool, which is above 4000 °C). Whereas, by applying lower heat input, the axial residual stress has a significant deviation from the shell and

the 2-D axisymmetric modeling. The most significant differences of these axial stresses results can be observed at the weld centerline, in which 3-D modeling with low heat input shows zero residual stress while the others already yielded at this point. On the other hand, by moving away from the centerline and closing to the heat affected zone boundary, it can be seen that the magnitude of axial stress in 3-D model with low energy input is going to a higher amount. Then after, all graphs get close to each other.

Exhibit 4-3 through 4-6 show the comparison results of hoop stresses and von Mises stresses at the inside and the outside of the stainless steel welded pipe. The hoop residual stress at the inside surface of pipe resulting from 3-D modeling with applied high-energy input is almost as the same as the 2-D axisymmetric and the shell results. As shown in Exhibit 4-3, the result of 3-D modeling of circumferential pipe welding with applied lower energy input is close to the results of the other graphs with a good approximation, but it shows a big difference in the weld centerline. It shows that it never approached to yielding stress of the base metal (Yield Strength for stainless steel 316L is 290 MPa).

On the other hand, the hoop stresses in the outside surface of the pipe in all three modeling methods do not have the same results in the welding area, as shown in Exhibit 4-4.

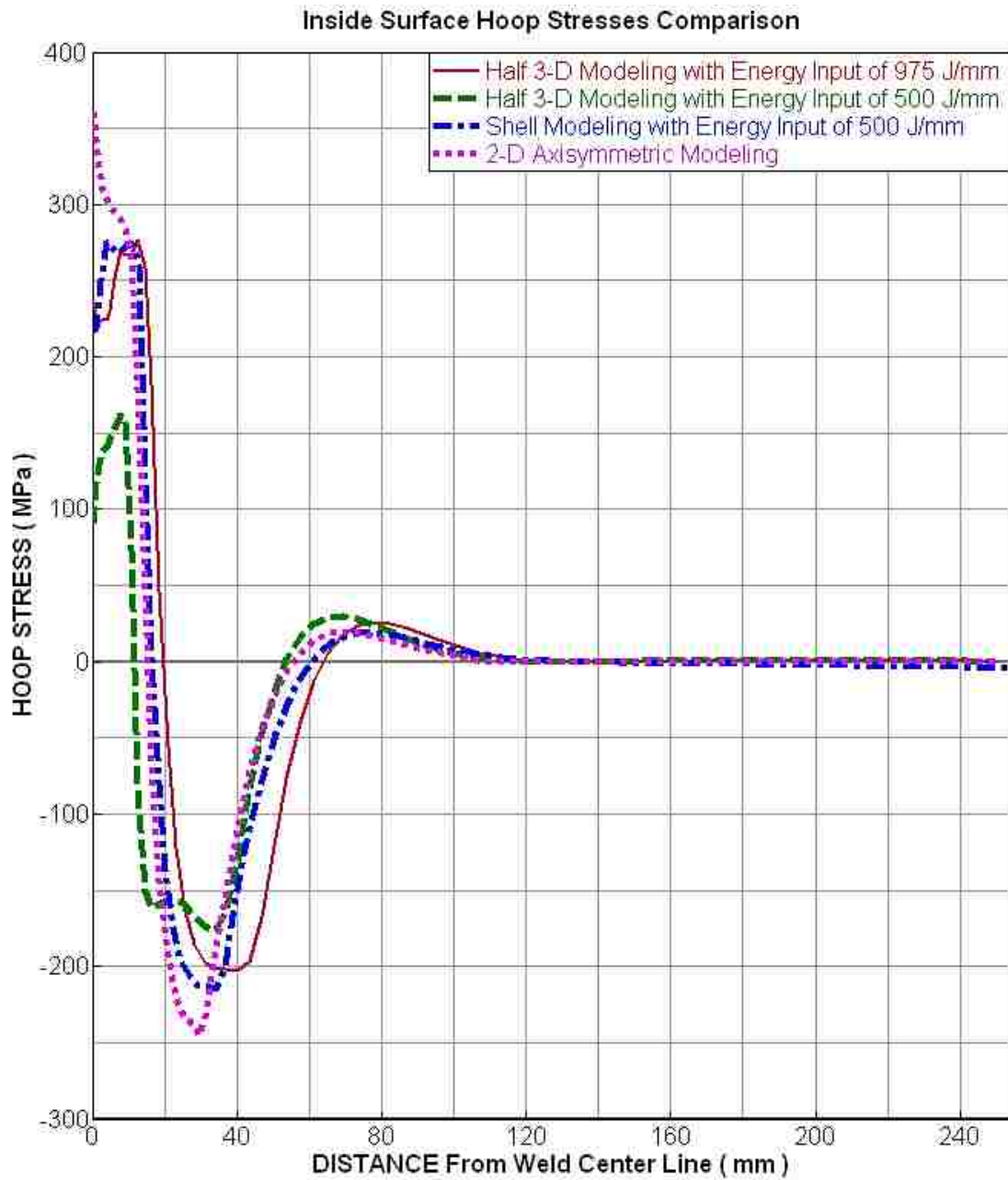


Exhibit 4-3 Comparison of hoop stresses at the inside surface of the pipe

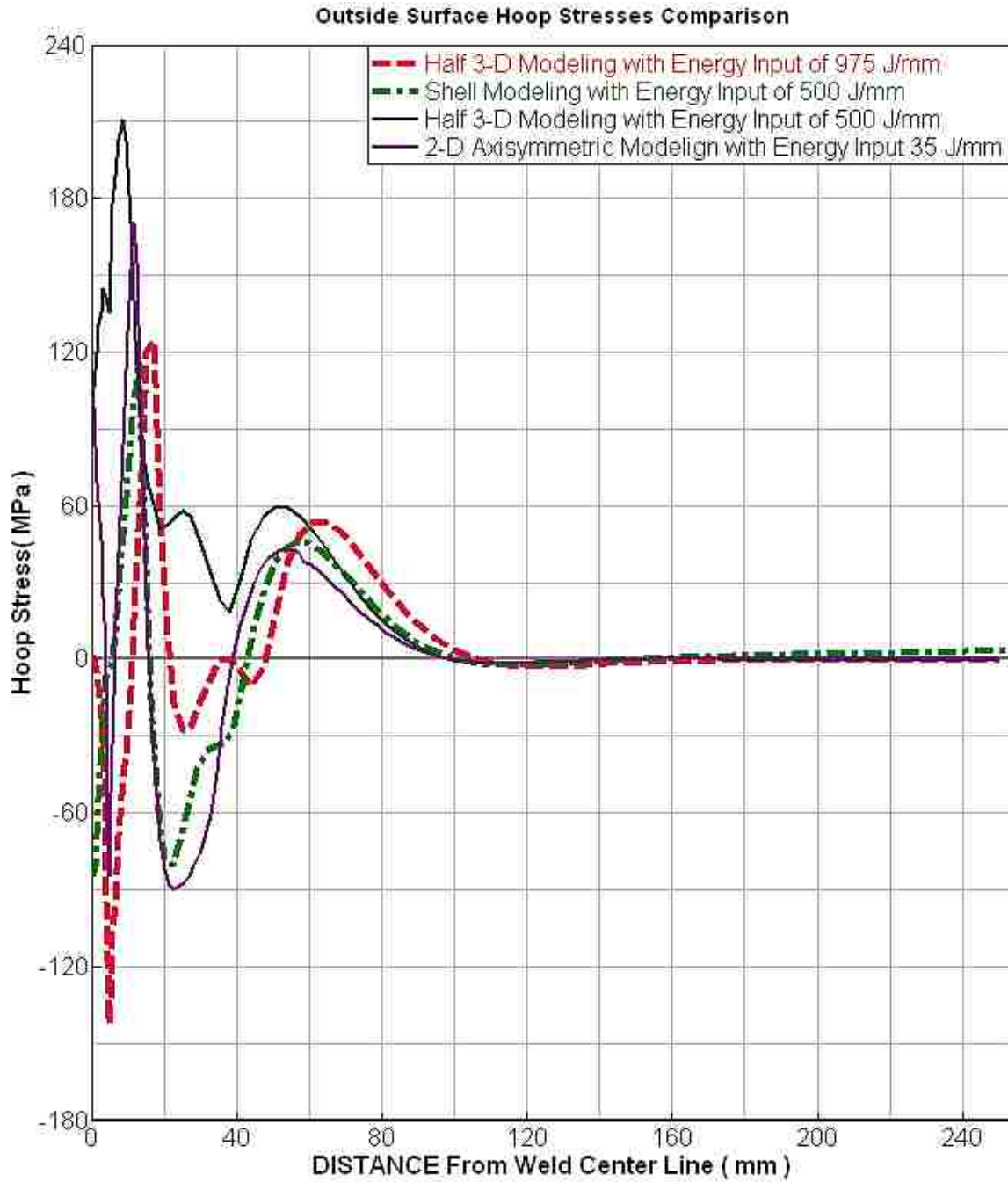


Exhibit 4-4 Comparison of hoop stresses at the outside surface of the welded pipe

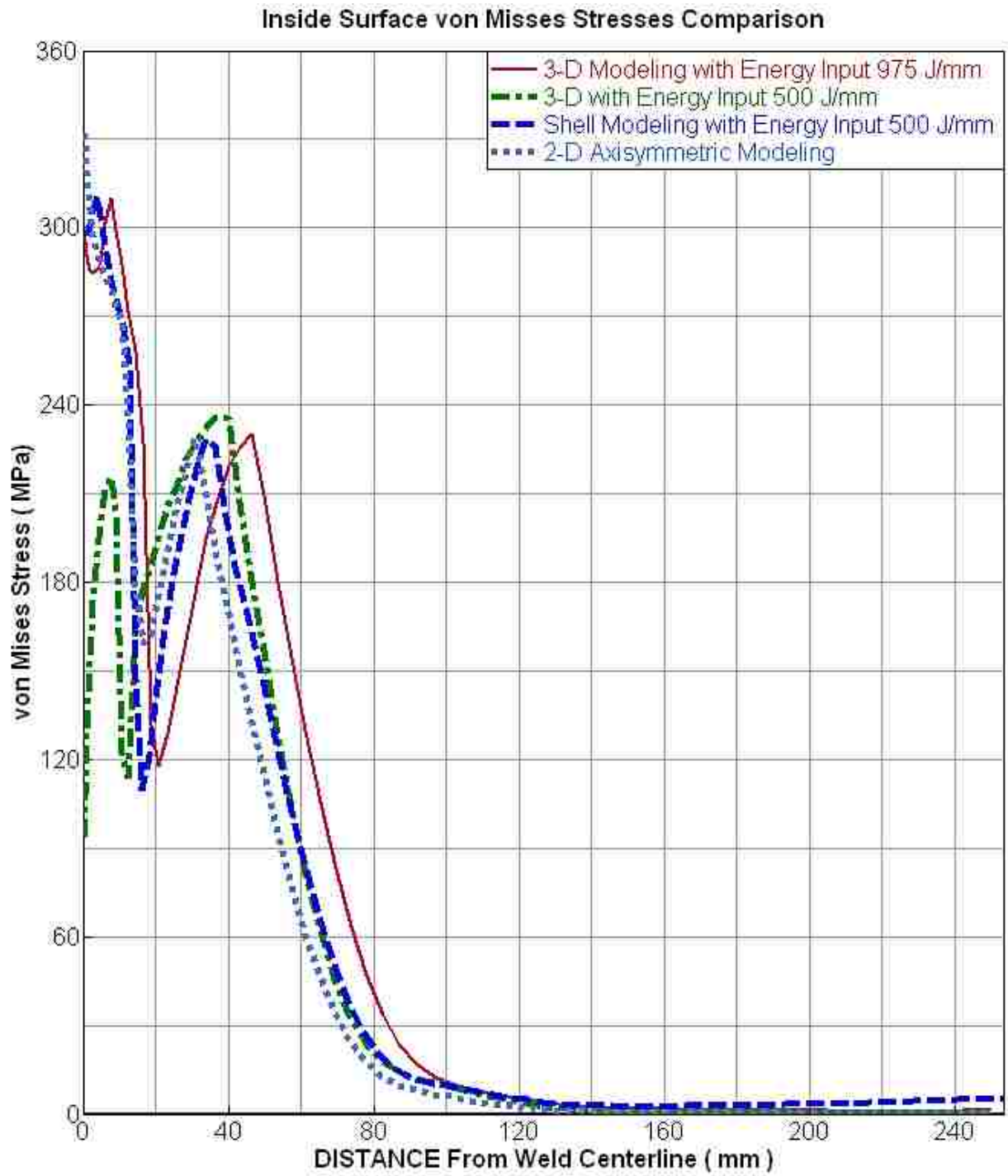


Exhibit 4-5 Comparison of von Mises stresses at the inside surface of the welded pipe

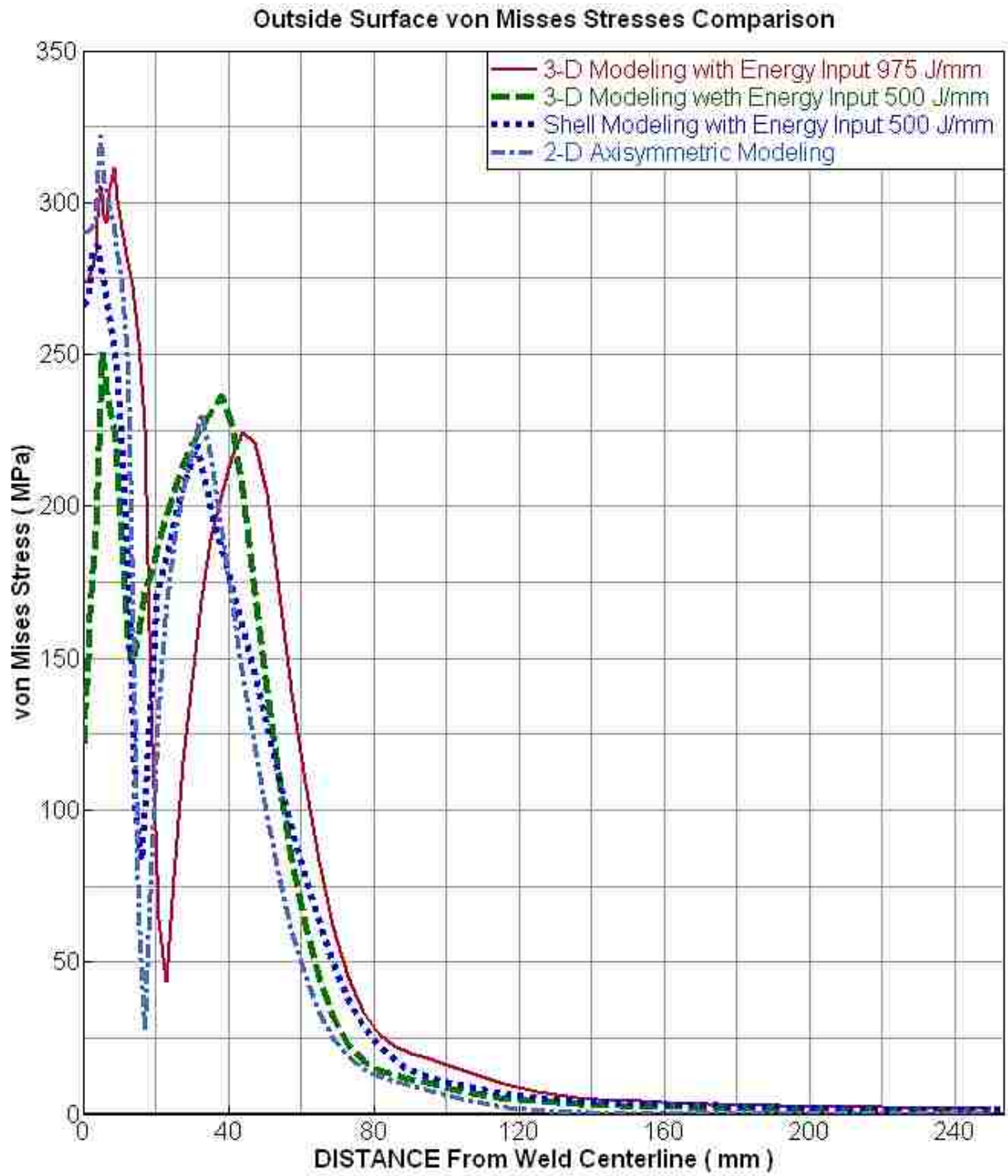


Exhibit 4-6 Comparison of von Mises stresses at the outside surface of the welded pipe

The results of von Mises stresses, as shown in Exhibit 4-5 and 4-6, for the inside and the outside of the pipe for all three modeling methods is the same as each other with a good approximation. However, the 3-D modeling with an applied lower energy input shows a significant difference in the welding area.

Another result that extracted from the simulation process is the investigation over influence of changing in the clamping conditions by applying different condition to the model and then compares the results. Exhibit 4-7 shows the effect of changing clamping condition over the residual axial stress in 2-D axisymmetric model.

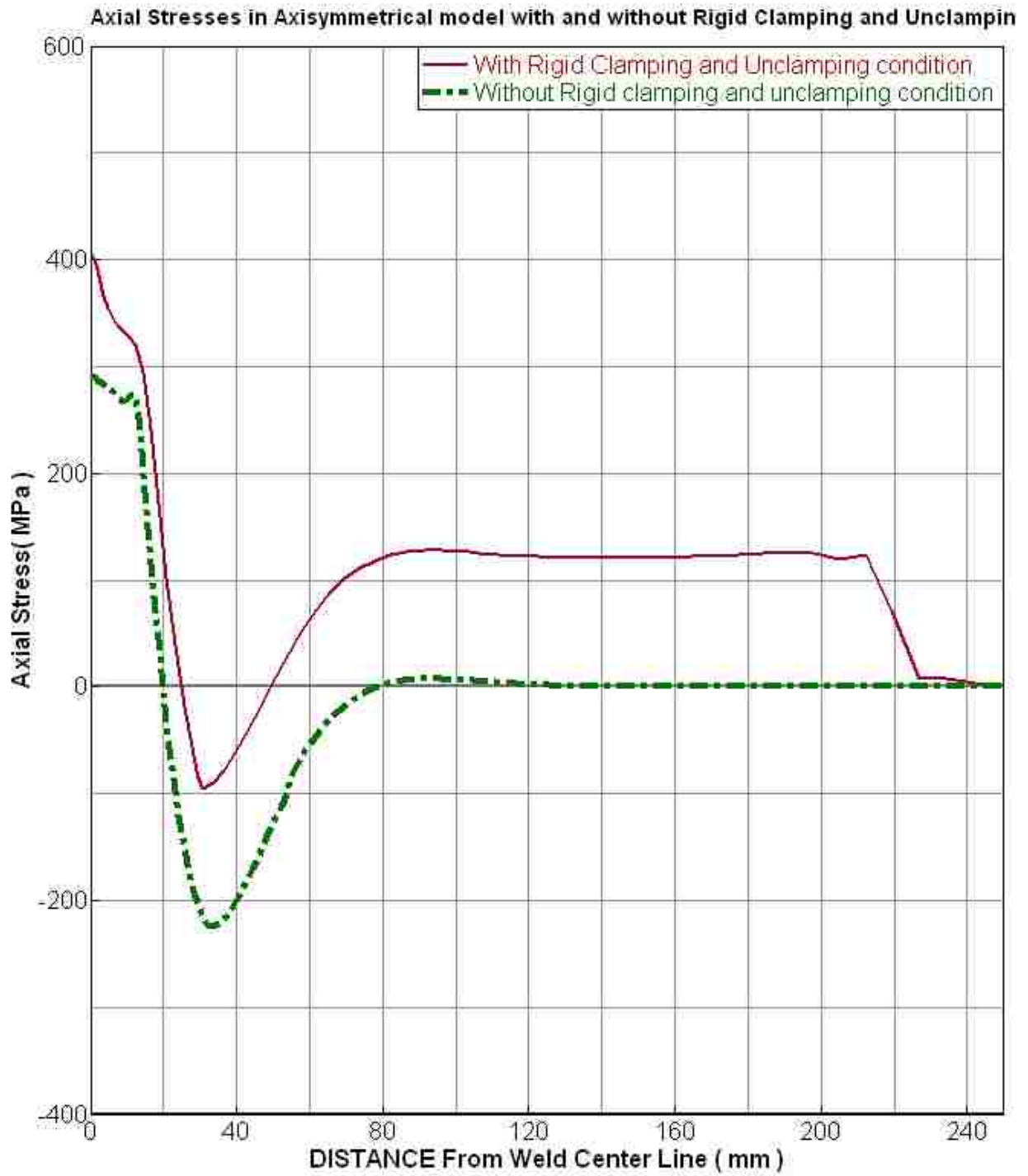


Exhibit 4-7 influence of clamping condition on axial residual stress in 2-D axisymmetric modeling

5 Conclusion and Future Works

To study the residual stresses due to circumferential girth welding of austenitic stainless steel pipe three-dimensional, 2-D axisymmetric and shell model simulations are performed using ESI Visual-Weld, ESI-Visual Mesh, and SYSWELD.

Based on the knowledge obtained during the work with the simulation of girth welding of stainless steel pipe, it is clear that the accuracy of welding simulations is largely dependent of the thermal and energy input.

According to the information obtained from section 4, effect of clamping condition is highly influenced on residual stresses due to welding.

Base on the information obtained from section 4 in associating with theory of heat source mentioned in section 2.2, show that effect of welding parameters, those directly influence on energy input, on the residual stresses are significant.

As a result of the welding process simulation using SYSWELD, it should be noted that all three modeling method cannot use the same values of welding parameters due to the effect of 3-D and circumferential welding.

By referring to von Mises diagrams in section 4, it can be seen that entering low energy input will result in no yielding in workpiece.

This study can be continued, at first step, by investigation over influence of other welding parameters in the all three simulation. The parameters such as:

- Effect of other welding methods

- Effect of radius to thickness ratio
- Effect of weld metal yield stress
- Effect of multi-pass welding

In addition, it is good for fatigue and fracture mechanics investigation to obtain DangVan criterion. By using these graph, the potential area for premature failure could be found.

Furthermore, the other welding applications could be developed by using the simulation process presented in this study, applications such as, welding of two dissimilar pipes, welding of pipes under external loading and other related applications.

6 References

- [1] E. Lima, J. Wagener, A. Pyzalla and T. Buslaps, "Investigations on Residual Stresses in Friction Stir Welds," in *3rd International Symposium on Friction Stir Welding*, Kobe, Japan, 2001.
- [2] M. Law, H. Prask, V. Luzin and T. Gnaeupel-Harold, "Residual stress measurements in coil, linepipe and girth welded pipe," Elsevier Science Ltd., Menai, 2006.
- [3] L. Karlsson, "RESIDUAL STRESSES DUE TO WELDING OF A NOZZLE TO A PRESSURE VESSEL," Lund University, Lund, 2005.
- [4] B. Brickstad and B. L. Josefson, "A parametric study of residual stresses in multi-pass butt-welded stainless steel pipes," Elsevier Science Ltd., Stockholm, 1995.
- [5] S. P. Timoshenko and S. Woinowsky-Krieger, *Theory of Plates and Shells*, 2 ed., New York: McGraw-Hill, 1959.
- [6] Michigan Occupational Safety and Health Administration, "ARC WELDING PROCESS," LARA Department of Licensing and Regulatory Affairs, Michigan, 2011.
- [7] Miller Electric Mfg. Co., "Guidelines For Shielded Metal Arc Welding (SMAW)," Miller Electric Mfg. Co., Appleton, 2013.
- [8] Miller Electric Mfg. Co., "Guidelines For Gas Metal Arc Welding," Appleton, 2012.
- [9] Miller Electric Mfg Co., "Submerged Arc Welding," Miller Electric Mfg Co., Appleton, 1982.
- [10] Miller Electric Mfg. Co., "Guidelines For Gas Tungsten Arc Welding," Appleton, 2012.
- [11] ESAB, "Plasma Arc Welding," ESAB Holding Ltd, 2013. [Online]. Available: <http://www.esab.com/global/en/education/processes-paw.cfm>. [Accessed 09 04 2013].
- [12] J. A. Goldak and M. Akhlaghi, *Computational Welding Mechanics*, Springer, 2005.
- [13] ESI Group, "USER Manual," ESI GROUP, 2012.
- [14] S. Kou, *Welding Metallurgy*, 2 ed., Hoboken, New Jersey: John Wiley & Sons, Inc., 2003.
- [15] D. Dean, S. Kiyoshima, H. Serizawa, H. Murakawa and Y. Horii, "Numerical Investigation on Welding Residual Stress in 2.25Cr-1Mo Steel Pipes," Joing and Welding Research Institute, Osaka, 2007.
- [16] N. U. Dar, E. M. Queshi and M. I. Himmouda, "Analysis of weld-induced residual stresses and distortion in thin-walled cylinders," Springer, 2009.

- [17] M. W. Lai, D. Rubin and E. Krempl, Introduction to Continuum Mechanics, 4th ed., Elsevier, 2010, pp. 184-185.
- [18] J. Goldak, M. Bibby, J. Moore, R. House and B. Patel, "Computer Modeling of Heat Flow in Welds," *Metallurgical Transactions B*, vol. 17, no. 3, pp. 587-600, September 1986.
- [19] C.-H. Lee and K.-H. Chang, "Prediction of residual stresses in high strength carbon steel pipe weld considering solid-state phase transformation effects," *Computers and Structures*, vol. 89, no. 1-2, pp. 256-265, 2011.
- [20] AK Steel, "316/316L STAINLESS STEEL Product Data Sheet," AK Steel, Ohio, 2007.
- [21] D. Kim, "Welding simulation of ship structures using coupled shell and solid volume finite elements," Lehigh University, Bethlehem, 2003.

Appendix A

Script Used in SYSWELD for Defining the Heat Source

NAME 3DMODGIRTWELDPPIPE_MESH_

SEARCH DATA 1000 ASCII

DEFINITION

3D Modeling of Circumferential Girth Welding of Pipe

OPTION THERMAL METALLURGY SPATIAL

RESTART GEOMETRY

MATERIAL PROPERTIES

ELEMENTS GROUPS \$PIPE\$ / MATE 1 STATUS -10000

ELEMENTS GROUPS \$FILLER\$ / MATE 1 STATUS -10000

MEDIUM

WELDLINE / GROUPS \$J01_PATH\$ REFERENCE \$J01_REF\$ ELEMENTS \$J01_SEL\$ START--

\$J01_SNO\$ ARRIVAL \$J01_ENO\$ VELOCITY 15.000188 TINF 0.000 MODEL 1

\$GROUP CREATE NAME GROUPNODEONLYYTRAJ

NODES 1 2

\$RETURN

CONSTRAINTS

ELEMENTS GROUPS \$AIR_HEAT_EXCHANGES\$ / KT 1 VARIABLE 1

LOAD

1

ELEMENTS GROUPS \$AIR_HEAT_EXCHANGES\$ / TT 20.000

ELEMENTS GROUPS \$WELDGROUP\$ / QR 1 VARIABLE -10001 TRAJECTORY 1

TABLE

1 / FORTRAN

function f(t)

c

c radiative losses : $f = \text{sig} * e * (t + \text{to})(t^{**2} + \text{to}^{**2})$

c

e = 0.8

sig = 5.67*-8

to = 20.

to = 20. + 273.15

t1 = t + 273.15

a = t1 * t1

b = to * to

c = a + b

d = t1 + to

d = d * c

d = d * e

d = d * sig

c

c convective losses = 25 W/m2

f = d + 25.

c change to W/mm2

d = 1*-6

f = f * d

c

return

END

10000 / FORTRAN

FUNCTION F(X)

DIMENSION X(4)

F = 1

RETURN

END

10001 / FORTRAN

C

C Normalized standard ARC Power source

C

C It needs only a weldline, no reference line. It is

C axial symmetric around the weldline

C

C The total absorbed power needs to be calibrated

C with an intensity function in the welding wizard

C or with the FIT block starting with V2008

C

C Power source dimensions see variables below

C

FUNCTION F(X)

C

DIMENSION X(4)

C

C Coordinates of the gauss point treated and time

C

$XX = X(1)$; X Coordinate

$YY = X(2)$; Y Coordinate

$ZZ = X(3)$; Z Coordinate

$TT = X(4)$; Time

C

C Parameters of the Goldak power source

C

C The absorbed power is defined within an ellipsoid

C

C Definition of the maximum front and rear power intensity

C

$QF = 1.0$; Normalized maximum front power source intensity

$QR = 0.833$; Normalized maximum rear power source intensity

C

C Definition of the measures of the Goldak ellipsoid

C They should be inside the molten zone

C

$AF = 5.000$; Front length of the molten zone

$AR = 10.000$; Rear length of the molten zone

C

C Width and depth

C

$B = 4.500$; Half of the width of the bead

$C = 9.000$; Penetration of the bead

C

C Position in space - completely handled by

C the welding wizzard - weldline

C

X0 = 0.0 ; X initial location of source center

Y0 = 0.0 ; Y initial location of source center

Z0 = 0.0 ; Z initial location of source center

VY = 0.0 ; Source displacement velocity

AY = 0.0 ; Angle of torch [deg.]

C

C Computation of the absorbed power

C

C F = QC * V1 * V2 * V3 with

C V1 = exp(-(YY-Y0-VY*TT)^2/AC^2)

C V2 = exp(-(XX-X0)^2/B^2)

C V3 = exp(-(ZZ-Z0)^2/C^2)

C if (-YY + Y0 +VY*TT) greater than 0

C QC = QF et AC = AF

C else

C QC = QR et AC = AR

C

C Constant

C

M1 = -1

PIDEG = ATAN(1.)

PIDEG = PIDEG / 45.

AY = AY * PIDEG

C

C Transformation of global to local coordinates

C

$$XD = XX - X0$$

$$YD = VY * TT$$

$$YD = YD + Y0$$

$$ZD = ZZ - Z0$$

C

C Source rotation about Y axis

C

$$SA = \text{SIN}(AY)$$

$$SA = -SA$$

$$CA = \text{COS}(AY)$$

$$A1 = XD * CA$$

$$A2 = ZD * SA$$

$$XL = A1 + A2$$

$$YL = YY - YD$$

$$A1 = ZD * CA$$

$$A2 = XD * SA$$

$$ZL = A1 - A2$$

C

C Condition computation, QC and AC initialisation

C

$$\text{COND} = VY * YL$$

$$\text{IF } (VY \text{ .EQ. } 0.) \text{ COND} = YL$$

$$QC = QR$$

$$AC = AR$$

IF(COND .GT. 0.) QC = QF

IF(COND .GT. 0.) AC = AF

C

C Vi computation

C

A1 = YL * YL

A2 = AC * AC

A2 = A1 / A2

A2 = M1 * A2

V1 = EXP(A2)

C

C V2 computation

C

A1 = XL * XL

A2 = B * B

A2 = A1 / A2

A2 = M1 * A2

V2 = EXP(A2)

C

C V3 computation

C

A1 = ZL * ZL

A2 = C * C

A2 = A1 / A2

A2 = M1 * A2

V3 = EXP(A2)

C

C F computation

C

F = QC * V1

F = F * V2

F = F * V3

C

RETURN

END

RETURN

NAME 3DMODGIRTWELDPIPE_

SAVE DATA 1000

Appendix B

Script Used in SYSWELD for Defining Mechanical Properties

NAME 3DMODGIRTWELDDPIPE_MESH_

SEARCH DATA 1000 ASCII

DEFINITION

3D Modeling of Circumferential Girth Welding of Pipe

OPTION THREEDIMENSIONAL THERMOELASTICITY

RESTART GEOMETRY

MATERIAL PROPERTIES

ELEMENTS GROUPS \$PIPE\$ / E -10000 NU 0.3 LX -10001 LY -10001 LZ -10001 --

YIELD -10002 SLOPE -10003 PHAS 2 TF 1400 AUST 2 KY -1 MODEL 3 STATUS -10004

ELEMENTS GROUPS \$FILLER\$ / E -10000 NU 0.3 LX -10001 LY -10001 LZ -10001 --

YIELD -10002 SLOPE -10003 PHAS 2 TF 1400 AUST 2 KY -1 MODEL 3 STATUS -10004

MEDIUM

WELDLINE / GROUPS \$J01_PATH\$ REFERENCE \$J01_REF\$ ELEMENTS \$J01_SEL\$ START--

\$J01_SNO\$ ARRIVAL \$J01_ENO\$ VELOCITY 15.000188 TINF 0.000 MODEL 1

\$GROUP CREATE NAME GROUPNODEONLYTRAJ

NODES 1 2

\$RETURN

CONSTRAINTS

NODES GROUPS \$CLMP_01\$ / UX UY UZ

PLANE PSI -90.0000 THETA 0.0000 PHI -20.2500 XX 0.0000 YY 249.9133 ZZ--

0.0000 / SYMMETRY

LOAD

1 NOTHING

TABLE

10000 / -10005 -10006

10001 / -10007 -10008

10002 / -10009 -10010

10003 / -10011 -10011

10004 / FORTRAN

FUNCTION F(X)

DIMENSION X(4)

F = 1

RETURN

END

10005 / 1 20 192372 100 185860 200 177720 300 169580 400 161440 500 153300

600 145100 700 137020 800 109766 900 63195 1000 37367 1100 16418

1200 10836 1300 8532 1400 859

10006 / 1 20 1000 1500 1000

10007 / 1 20 0 100 0.00123 200 0.00292 300 0.00472 400 0.0066 500 0.00853

600 0.0105 700 0.0125 800 0.0146 900 0.0167 1000 0.0189 1100 0.0211

1200 0.0234 1300 0.0256 1400 0.0279

10008 / 1 0 0 1500 0

10009 / 1 20 275 100 238 200 198 300 172 400 157 500 151 600 145 700

136 800 127 900 115 1000 78 1100 38 1200 24 1300 16 1400 2

10010 / 1 20 275 100 238 200 198 300 172 400 157 500 151 600 145 700

136 800 127 900 115 1000 78 1100 38 1200 24 1300 16 1400 2

10011 / 7 20 10012 100 10013 200 10014 300 10015 400 10016 500 10017

600 10018 700 10019 800 10020 900 10021 1000 10022 1100 10023 1200 10024 1300 10025 1400
10026

10012 / 1 0 0 0.2 286
10013 / 1 0 0 0.2 252
10014 / 1 0 0 0.2 269
10015 / 1 0 0 0.2 279
10016 / 1 0 0 0.2 278
10017 / 1 0 0 0.2 268
10018 / 1 0 0 0.2 242
10019 / 1 0 0 0.2 204
10020 / 1 0 0 0.2 166
10021 / 1 0 0 0.2 54
10022 / 1 0 0 0.2 22
10023 / 1 0 0 0.2 6
10024 / 1 0 0 0.2 5
10025 / 1 0 0 0.2 7
10026 / 1 0 0 0.2 0.1

RETURN

NAME 3DMODGIRTWELDPipe_

SAVE DATA 2000

MEDIUM

EXTRACT MEDIUM

Vita

Farzan Tarak was born on February 14, 1974 in Iran. His hometown is Abadan located in south west of Iran. He grew up in Karaj since left his hometown due to Iran-Iraq War in 1981. He has married in 2002 with Elham Takin. He has been in Lehigh University since 2012 as a Master of Science student in the department of mechanical engineering, studied solid mechanics. He was working with Professor Herman F. Nied concentrating on computerized simulation of welding process in order to define new concepts in this field of study.

Before studied at Lehigh University, Farzan received his Bachelor of Science in mechanical engineering at Azad University of Karaj, Iran, in 1999. During his attendance in Azad University, he did his first research as a senior project, “Computerized Simulation of Internal Combustion Engine & Applying and Analyzing the Linear Controllers on the System.”

After graduation, he decided to join a dynamic company to utilize his talents. Therefore, he started with a fabrication company as an engineering manager in 1999 and then after he worked for two different companies in position of project engineer in two capital industrial projects in mining, cement, and manufacturing fields between 2003 to 2008.

Farzan also accomplished some personal projects between 2006 and 2008 in fields of mining and cement industry for Mobarakeh Steel Co. and Mazandaran Cement Co.

After completion of his project in 2008, Fabrication and installation of Extension Line & Upgrading Project in Neka Cement Plant, he decided to leave his home country to the USA looked for the opportunity of having professional education and research. Farzan got a graduate school admission at Temple University in 2010 in the major of mechanical engineering, but he decided to transfer to Lehigh University in spring 2012, to satisfy his professional goals and his fields of study.